the manufacturer's instructions. A comprehensive expression analysis was performed using 2 μg of total RNA from each sample and GeneChip® Human Genome U133 plus 2.0 probe arrays (Affymetrix, Santa Clara, CA) according to the manufacturer's instructions. To normalize the variations in staining intensity among chips, the 'Signal' values for all probes on a given chip were divided by the median value for expression of all genes on the chip. To consider genes containing only a background signal, probes were eliminated only if the 'Signal' value was less than 10, or the Detection call was 'Absent' in any sample using GeneSpring software version 7.2 (Agilent Technologies, Palo Alto). The gene chip analysis was carried out on 8 independent scleral cultures.

Hierarchical clustering and principal component analysis (PCA)

To analyze the gene expression data in an unsupervised manner by gene chip array, we used hierarchical clustering and principal component analysis (NIA Array; http://lgsun.grc.nia.nih.gov/ANOVA/ [27], TIGR MeV; http://www.tm4.org/mer.html [28]). The hierarchical clustering techniques classify data by similarity and the results are represented by dendrogram. PCA is a multivariate analysis technique which finds major patterns in data variability. Hierarchical clustering and PCA were performed on the data of gene chip analysis (a single assay for each sample) to group scleral cells and other mesenchymal cells into subcategories (Table 1).

In vitro chondrogenesis

Two hundred thousand scleral cells were placed in a 15-ml polypropylene tube (Becton Dickinson) and centrifuged for 10 minutes. The pellet was cultured in DF-C medium™ containing 0.1 μM dexamethasone, 1 mM sodium pyruvate, 0.17 mM ascorbic acid-2-phosphate, 0.35 mM proline, 6.25 μg/ml bovine insulin, 6.25 μg/ml transferrin, 6.25 μg/ml selenous acid, 5.33 μg/ml linoleic acid, 1.25 mg/ml BSA, 5 ng/ml TGF-β1, 5 ng/ml BMP2, and 3% fetal bovine serum (TOYOBO). The medium was replaced every 3 to 4 days for 28 days. For microscopy, the pellets were embedded in paraffin, cut into 5-μm sections, and stained with alcian blue [29,30].

In vivo chondrogenesis

Under anesthesia, full thickness cartilage defects were created in the trochlear groove of the femur in SD rats. The defects were filled with DiI-labeled human scleral cells. The rats were returned to their cages after the operation and allowed to move freely. Animals were sacrificed with an overdose of sodium pentobarbital at 4 weeks after the operation. Specimens were dissected and embedded in paraffin. The sections were stained with toluidine blue and immunohistochemically stained with anti-type II collagen antibodies (clone F-57, DAIICHI FINE CHEMICAL, Co. Ltd., Toyama, Japan). All animals received humane care in compliance with the "Principles of Laboratory Animal Care" formulated by the National Society for Medical Research and the "Guide for the Care and Use of Laboratory Animals" prepared by the Institute of Laboratory Animal Resources and published by the US National Institutes of Health (NIH Publication No. 86-23, revised 1985). The operation protocols were accepted by the Laboratory Animal Care and Use Committee of the Research Institute for Child and Health Development (2003-002).

Reverse transcriptase-PCR

Total RNA was isolated with an RNeasy Plus mini-kit. Cartilage pellets were digested with 3 mg/ml Collagenase D for 3 hours at 37°C.

The following PCR primer sets were used for cartilage-associated genes: aggrecan, sense (5′-TACACTGGCGAGCACTGTAAC -3′) and antisense (5′-CAGTGGCCCTGGTACTTGTT-3′), product size, 71 bp; collagen, type II, alpha 1, sense (5′-TTCAGCTATG-GAGATGACAATC -3′) and antisense (5′-AGAGTCCTAGAGT-GACTGAG -3′), product size, 472 bp; collagen, typeX, alpha 1, sense (5′-CACCTTCTGCACTGCTCATC-3′) and antisense (5′-GGCAGCATATTCTCAGATGGA-3′), product sizem, 104 bp; SOX5, sense (5′-AGCCAGAGTTAGCACAATAGG -3′) and antisense (5′-CATGATTGCCTTGTATTC -3′), product size, 619 bp; SOX6, sense (5′-ACTGTGGCTGAAGCACGAGTC -3′) and antisense (5′-TCCGCCATCTGTCTTCATACC -3′), product size, 562 bp; SOX9, sense (5′-GTACCCGCACTTGCACAAC-3′) and antisense (5′-TCGCTCTCGTTCAGAAGTCTC-3′), product size 72 bp; Indian hedgehog homolog (IHH), sense (5′-TGCATTGCT-CCGTCAAGTC-3′) and antisense (5′-CCACTCTCCAGGCG-TACCT-3′), product size 88 bp; parathyroid hormone receptor 1(PTHR1), sense (5′-CCTGAGTCTGAGGAGGACAAG-3′) and antisense (5′-CACAGGATGTGGTCCCATT-3′), product size 86 bp; matrix metallopeptidase 13 (MMP13), sense (5′-CCAGTCTCC-GAGGAGAAACA-3′) and antisense (5′-AAAAACAGCTCCG-CATCAAC-3′),product size, 85 bp, and GAPDH, sense (5′-GCTCAGACACCATGGGGAAGGT-3′) and antisense (5′-GTGGTGCAGGAGGCATTGCTGA-3′), product size, 474 bp.

Supporting Information

Figure S1 Global gene expression analysis of cultured human cells. Hierarchical clustering analysis based on expression levels of the cartilage-associated genes (NIA Array Analysis). We performed gene chip analysis (a single assay for each analysis) for eight independent primary scleral cultures from five patients (donors). We started eight independent cultures from three different scleral sites of Donor 2 (e.g. the anterior site 1.5 mm apart from the limbs, the middle part, and the posterior part), 2 different scleral sites of Donor 5, and three scleral sites of Donor 1, 3, and 4. We performed hierarchical clustering analysis, using these independent cultures and obtained consistent results, that is, "sclera"-derived cells are categorized into one sub-group. Furthermore, the sclera, cartilage, synovium, and joint fluid are categorized into the same group.

Found at: doi:10.1371/journal.pone.0003709.s001 (0.07 MB PDF)

Figure S2 Cartilage-associated gene expressions in cultured fibroblasts derived from the dermis and the sclera. Cartilage-associated gene expressions by RT-PCR in cultured fibroblasts derived from the dermis and the sclera. Aggrecan, COL2A, IHH and PTHR mRNA expressions were clearly stronger in the scleral fibroblasts compared to the dermal fibroblasts, indicating that chondrogenic nature could be specific for the sclera among collagenous tissues.

Found at: doi:10.1371/journal.pone.0003709.s002 (0.01 MB PDF)

Table S1 Cartilage-associated genes

Found at: doi:10.1371/journal.pone.0003709.s003 (0.01 MB PDF)

Acknowledgments

We would like to express our sincere thanks to T. Tang for helping with animal experiments and T. Sugiki, M. Nasu, A. Kawakita and M. Toyoda for their discussion of this work.

Author Contributions

Conceived and designed the experiments: YS NA TM IS AU. Performed the experiments: YS NA HM TM IS. Analyzed the data: YS YT KM HS IS. Contributed reagents/materials/analysis tools: YS NA IS. Wrote the paper: YS KM HS IS AU.

References

1. Connon CJ, Meek KM, Kinoshita S, Quantock AJ (2004) Spatial and temporal alterations in the collagen fibrillar array during the onset of transparency in the avian cornea. Exp Eye Res 78: 909–913.
2. Yoshida S, Shimmura S, Shimazaki J, Shinozaki N, Tsubota K (2005) Serum-free spheroid culture of mouse corneal keratocytes. Invest Ophthalmol Vis Sci 46: 1653–1658.
3. Zhou J, Rappaport EF, Tobias JW, Young TL (2006) Differential gene expression in mouse sclera during ocular development. Invest Ophthalmol Vis Sci 47: 1794–1802.
4. Young TL, Guo XD, King RA, Johnson JM, Rada JA (2003) Identification of genes expressed in a human scleral cDNA library. Mol Vis 9: 508–514.
5. Sakaguchi Y, Sekiya I, Yagishita K, Muneta T (2005) Comparison of human stem cells derived from various mesenchymal tissues: superiority of synovium as a cell source. Arthritis Rheum 52: 2521–2529.
6. Yoshimura H, Muneta T, Nimura A, Yokoyama A, Koga H, et al. (2007) Comparison of rat mesenchymal stem cells derived from bone marrow, synovium, periosteum, adipose tissue, and muscle. Cell Tissue Res 327: 449–462.
7. Koga H, Muneta T, Ju YJ, Nagase T, Nimura A, et al. (2007) Synovial stem cells are regionally specified according to local microenvironments after implantation for cartilage regeneration. Stem Cells 25: 689–696.
8. Seko Y, Shimokawa H, Tokoro T (1995) Expression of bFGF and TGF-beta 2 in experimental myopia in chicks. Invest Ophthalmol Vis Sci 36: 1183–1187.
9. Seko Y, Tanaka Y, Tokoro T (1995) Influence of bFGF as a potent growth stimulator and TGF-beta as a growth regulator on scleral chondrocytes and scleral fibroblasts in vitro. Ophthalmic Res 27: 144–152.
10. Franz-Odendaal TA, Hall BK (2006) Skeletal elements within teleost eyes and a discussion of their homology. J Morphol 267: 1326–1337.
11. Archer CW, McDowell J, Bayliss MT, Stephens MD, Bentley G (1990) Phenotypic modulation in sub-populations of human articular chondrocytes in vitro. J Cell Sci 97 (Pt 2): 361–371.
12. Hauselmann HJ, Fernandes RJ, Mok SS, Schmid TM, Block JA, et al. (1994) Phenotypic stability of bovine articular chondrocytes after long-term culture in alginate beads. J Cell Sci 107 (Pt 1): 17–27.
13. Reginato AM, Iozzo RV, Jimenez SA (1994) Formation of nodular structures resembling mature articular cartilage in long-term primary cultures of human fetal epiphyseal chondrocytes on a hydrogel substrate. Arthritis Rheum 37: 1338–1349.
14. Benya PD, Shaffer JD (1982) Dedifferentiated chondrocytes reexpress the differentiated collagen phenotype when cultured in agarose gels. Cell 30: 215–224.
15. Bonaventure J, Kadhom N, Cohen-Solal L, Ng KH, Bourguignon J, et al. (1994) Reexpression of cartilage-specific genes by dedifferentiated human articular chondrocytes cultured in alginate beads. Exp Cell Res 212: 97–104.
16. Lefebvre V, Peeters-Joris C, Vaes G (1990) Production of collagens, collagenase and collagenase inhibitor during the dedifferentiation of articular chondrocytes by serial subcultures. Biochim Biophys Acta 1051: 266–275.
17. Pittenger MF, Mackay AM, Beck SC, Jaiswal RK, Douglas R, et al. (1999) Multilineage potential of adult human mesenchymal stem cells. Science 284: 143–147.
18. Shukunami C, Shigeno C, Atsumi T, Ishizeki K, Suzuki F, et al. (1996) Chondrogenic differentiation of clonal mouse embryonic cell line ATDC5 in vitro: differentiation-dependent gene expression of parathyroid hormone (PTH)/PTH-related peptide receptor. J Cell Biol 133: 457–468.
19. Lefebvre V, Li P, de Crombrugghe B (1998) A new long form of Sox5 (L-Sox5), Sox6 and Sox9 are coexpressed in chondrogenesis and cooperatively activate the type II collagen gene. Embo J 17: 5718–5733.
20. Sekiya I, Tsuji K, Koopman P, Watanabe H, Yamada Y, et al. (2000) SOX9 enhances aggrecan gene promoter/enhancer activity and is up-regulated by retinoic acid in a cartilage-derived cell line, TC6. J Biol Chem 275: 10738–10744.
21. Kobayashi T, Soegiarto DW, Yang Y, Lanske B, Schipani E, et al. (2005) Indian hedgehog stimulates periarticular chondrocyte differentiation to regulate growth plate length independently of PTHrP. J Clin Invest 115: 1734–1742.
22. Jayson MI, Jones DE (1971) Scleritis and rheumatoid arthritis. Ann Rheum Dis 30: 343–347.
23. Barr CC, Davis H, Culbertson WW (1981) Rheumatoid scleritis. Ophthalmology 88: 1269–1273.
24. Isaak BL, Liesegang TJ, Michet CJ Jr (1986) Ocular and systemic findings in relapsing polychondritis. Ophthalmology 93: 681–689.
25. Annunen S, Korkko J, Czarny M, Warman ML, Brunner HG, et al. (1999) Splicing mutations of 54-bp exons in the COL11A1 gene cause Marshall syndrome, but other mutations cause overlapping Marshall/Stickler phenotypes. Am J Hum Genet 65: 974–983.
26. Van Camp G, Snoeckx RL, Hilgert N, van den Ende J, Fukuoka H, et al. (2006) A new autosomal recessive form of Stickler syndrome is caused by a mutation in the COL9A1 gene. Am J Hum Genet 79: 449–457.
27. Sharov AA, Dudekula DB, Ko MS (2005) A web-based tool for principal component and significance analysis of microarray data. Bioinformatics 21: 2548–2549.
28. Saeed AI, Sharov V, White J, Li J, Liang W, et al. (2003) TM4: a free, open-source system for microarray data management and analysis. Biotechniques 34: 374–378.
29. Sugiki T, Uyama T, Toyoda M, Morioka H, Kume S, et al. (2007) Hyaline cartilage formation and enchondral ossification modeled with KUM3 and OP9 chondroblasts. J Cell Biochem 100: 1240–1254.
30. Sekiya I, Larson BL, Vuoristo JT, Reger RL, Prockop DJ (2005) Comparison of effect of BMP-2, -4, and -6 on in vitro cartilage formation of human adult stem cells from bone marrow stroma. Cell Tissue Res 320: 269–276.
31. Morito T, Muneta T, Hara K, Ju YJ, Mochizuki T, et al. (2008) Synovial fluid-derived mesenchymal stem cells increase after intra-articular ligament injury in humans. Rheumatology (Oxford) 47: 1137–1143.
32. Segawa Y, Muneta T, Makino M, Nimura A, Mochizuki T, et al. (in press) Mesenchymal stem cells derived from synovium, meniscus, anterior cruciate ligament, and articular chondrocytes share similar gene expression profiles. Journal of Orthopaedic Research.
33. Tsuruga Y, Kiyono T, Matsushita M, Takahashi T, Kami N, et al. (2008) Effect of intrasplenic transplantation of immortalized human hepatocytes in the treatment of acetaminophen-induced acute liver failure SCID mice. Transplant Proc 40: 617–619.
34. Mochizuki T, Muneta T, Sakaguchi Y, Nimura A, Yokoyama A, et al. (2006) Higher chondrogenic potential of fibrous synovium- and adipose synovium-derived cells compared with subcutaneous fat-derived cells: distinguishing properties of mesenchymal stem cells in humans. Arthritis Rheum 54: 843–853.

OPEN ACCESS Freely available online

PLoS one

Nicotine Acts on Growth Plate Chondrocytes to Delay Skeletal Growth through the α7 Neuronal Nicotinic Acetylcholine Receptor

Atsuo Kawakita[1,2], Kazuki Sato[2], Hatsune Makino[1], Hiroyasu Ikegami[2], Shinichiro Takayama[3], Yoshiaki Toyama[2], Akihiro Umezawa[1]*

1 Department of Reproductive Biology, National Institute for Child Health and Development, Tokyo, Japan, 2 Department of Orthopaedic Surgery, Keio University School of Medicine, Tokyo, Japan, 3 Department of Orthopaedic Surgery, National Center for Child Health and Development, Tokyo, Japan

Abstract

Background: Cigarette smoking adversely affects endochondral ossification during the course of skeletal growth. Among a plethora of cigarette chemicals, nicotine is one of the primary candidate compounds responsible for the cause of smoking-induced delayed skeletal growth. However, the possible mechanism of delayed skeletal growth caused by nicotine remains unclarified. In the last decade, localization of neuronal nicotinic acetylcholine receptor (nAChR), a specific receptor of nicotine, has been widely detected in non-excitable cells. Therefore, we hypothesized that nicotine affect growth plate chondrocytes directly and specifically through nAChR to delay skeletal growth.

Methodology/Principal Findings: We investigated the effect of nicotine on human growth plate chondrocytes, a major component of endochondral ossification. The chondrocytes were derived from extra human fingers. Nicotine inhibited matrix synthesis and hypertrophic differentiation in human growth plate chondrocytes in suspension culture in a concentration-dependent manner. Both human and murine growth plate chondrocytes expressed alpha7 nAChR, which constitutes functional homopentameric receptors. Methyllycaconitine (MLA), a specific antagonist of alpha7 nAChR, reversed the inhibition of matrix synthesis and functional calcium signal by nicotine in human growth plate chondrocytes in vitro. To study the effect of nicotine on growth plate in vivo, ovulation-controlled pregnant alpha7 nAChR +/− mice were given drinking water with or without nicotine during pregnancy, and skeletal growth of their fetuses was observed. Maternal nicotine exposure resulted in delayed skeletal growth of alpha7 nAChR +/+ fetuses but not in alpha7 nAChR −/− fetuses, implying that skeletal growth retardation by nicotine is specifically mediated via fetal alpha7 nAChR.

Conclusions/Significance: These results suggest that nicotine, from cigarette smoking, acts directly on growth plate chondrocytes to decrease matrix synthesis, suppress hypertrophic differentiation via alpha7 nAChR, leading to delayed skeletal growth.

Citation: Kawakita A, Sato K, Makino H, Ikegami H, Takayama S, et al. (2008) Nicotine Acts on Growth Plate Chondrocytes to Delay Skeletal Growth through the α7 Neuronal Nicotinic Acetylcholine Receptor. PLoS ONE 3(12): e3945. doi:10.1371/journal.pone.0003945

Editor: Rory Edward Morty, University of Giessen Lung Center, Germany

Received August 6, 2008; **Accepted** November 8, 2008; **Published** December 16, 2008

Funding: This study was supported by a grant from the Smoking Research Foundation; by grants from the Ministry of Education, Culture, Sports, Science, and Technology (MEXT) of Japan; by the Ministry of Health, Labour and Welfare (MHLW) Sciences Research Grants; by a Research Grant on Health Science focusing on Drug Innovation from the Japan Health Science Foundation; by the program for promotion of Fundamental Studies in Health Science of the Pharmaceuticals and Medical Devices Agency; by a Research Grant for Cardiovascular Disease from the MHLW; and by a Grant for Child Health and Development from the MHLW. The funders had no role in study design, data collection and analysis, decision to publish, or preparation of the manuscript.

Competing Interests: The authors have declared that no competing interests exist.

* E-mail: umezawa@1985.jukuin.keio.ac.jp

Introduction

Though detrimental effects of cigarette smoking to the human body have been widely demonstrated, the effects on endochondral ossification are not well understood. Epidemiologically, maternal smoking reduces the height of newborns [1–3]. However, there are controversial views regarding the mechanisms behind delayed skeletal growth caused by cigarette smoking. The socioeconomic status of smoking mothers [6,7], deficient maternal diet [8], chronic hypoxia caused by carbon monoxide [9], impaired placental size and function, and decreased blood flow of placenta caused by nicotine [10] have all been reported as a possible causal factors responsible for reduction in height of newborns. Conversely, it has also been reported that socioeconomic status [11], maternal diet [12], and hypoxia are not responsible for the cause of delayed skeletal growth. Research suggests that smoking not only reduces body length but also brings ossification retardation in the rat smoking model [13]. Moreover, smoking delays chondrogenesis in a mouse model of fracture healing [14]. Cigarette smoking, thus, adversely affects endochondral ossification somehow during the course of skeletal growth and repair in animal models.

Among a multitude of chemicals and physiological functions arising from cigarette smoking, nicotine is one of the leading candidates for causing small newborns. Epidemiologically, nicotine content in cigarette is related to reduced birth length in humans [15]. However, the possible mechanism of delayed skeletal growth caused by nicotine remains unclarified. In this study, we investigated the effect of nicotine on growth plate chondrocytes, the principle

component of endochondral ossification. In the last decade, localization of neuronal nicotinic acetylcholine receptor (nAChR), a specific receptor of nicotine, has been widely detected in non-excitable cells [16]. Therefore, we hypothesized that nicotine affect growth plate chondrocytes directly and specifically through nAChR to delay skeletal growth. We here demonstrate that nicotine affected growth plate chondrocytes through alpha7 nAChR to decrease matrix synthesis and to suppress hypertrophic differentiation, thereby delaying skeletal growth.

Results

Detection and localization of nAChR in growth plate chondrocytes

To date, many epidemiological [1–5] and experimental [13] studies suggested that endochondral ossification is affected by cigarette smoking, especially by its major component, nicotine [15]. We thus assumed that nicotine may directly affect chondrocytes, a key player in endochondral ossification. To investigate whether the impact of nicotine on chondrocytes is specific, we studied the expression pattern of the specific receptor, nAChR. For screening of the existing subunits of nAChR, RT-PCR was performed with primers for each subunit of nAChR. Human growth plate chondrocytes expressed alpha5, alpha7, beta1 and epsilon subunits of nAChR (Figure 1A).

Among the detected subunits, only the alpha7 subunit can form a functional nAChR by forming a homopentameric receptor [17]. We thus tried to detect alpha7 subunit at a protein level. Western blot analysis revealed that chondrocytes produced alpha7 nAChR (Figure 1B). Immunocytochemical analysis also revealed that chondrocytes stained positive for alpha7 nAChR (Figure 1C). Moreover, the alpha7 subunit was detected at resting, proliferating and pre-hypertrophic chondrocytes of murine growth plate but not hypertrophic chondrocytes (Figure 1D). These results suggest that the growth plate chondrocytes in their non-hypertrophic stage express alpha7 homopentameric nAChR.

Effect of nicotine on chondrocytes cultured in agarose gel

To study the effect of nicotine on growth plate chondrocytes in vitro, two methods of suspension cultures, i.e., agarose gel culture and alginate bead culture, were employed. In agarose gel, the chondrocytes are initially embedded in the suspension layer solitarily. The chondrocytes then proliferate, differentiate, and aggregate to form a colony in the presence of ascorbic acid, and start to produce a matrix around themselves [18]. We applied the agarose gel culture to study the effect of nicotine on the proliferation and differentiation of growth plate chondrocytes in vitro. Nicotine was added to culture media for three weeks culture period. Nicotine decreased the percentage of colonies which produce matrix, as revealed by alcian blue (ALB) stains in a concentration-dependent manner (Figure 2A, upper panels). Similarly, nicotine suppressed Col X expression and enzyme activity of alkaline phosphatase (ALP) in a concentration-dependent manner (Figure 2A, middle and lower row panels). In contrast, nicotine did not affect colony density (Figure 2B, left panel) or the number of cells per colony (Figure 2B, right panel) which are indicators for cell proliferation. No nicotinic effect on cell proliferation was detected as assessed by immunohistochemistry using antibody to proliferating cell nuclear antigen (PCNA) (Figure S1). These results suggest that nicotine decreases the matrix synthesis and suppresses hypertrophic differentiation of growth plate chondrocytes, but has little effect on cell proliferation in vitro and vivo. To investigate if the nicotinic effect is mediated by alpha7 nAChR, we used MLA, the specific antagonist of alpha7 nAChR. MLA clearly reversed the effect, as assessed by ALB-stained colonies (Figure 2C), suggesting the involvement of alpha7 nAChR in the effect of nicotine on growth plate chondrocytes.

Long-term (four months) effect of nicotine on growth plate chondrocytes in alginate beads

Different from the case with agarose gel, human chondrocytes hardly proliferate in alginate beads, maintaining chondrocyte properties for more than eight months [19]. Moreover, molecular analysis can be done easily compared with that in agarose gel, since chondrocytes can be recovered from beads by chelation of divalent ions with ethylenediamine tetraacetic acid (EDTA) followed by centrifugation. We investigated the long-term effect of nicotine on growth plate chondrocytes by employing alginate bead culture. Chondrocytes encapsulated in alginate beads remained viable during the culture period (four months) in their lacunae. Nicotine did not affect viability of the chondrocytes at any indicated concentration. Nicotine dose-dependently suppressed ALB- and Safranin-O-stained areas at four months (Figure 3A).

To investigate expression of chondrocyte-specific genes, we performed RT-PCR analysis on chondrocytes in alginate beads. Genes for collagen type II (Col II), Aggrecan, collagen type X (ColX), ALP, and indian hedgehog (Ihh) were up-regulated at three weeks after the start of alginate bead culture (Figure 3B). In contrast, genes for parathyroid hormone receptor type I (PTHR1), matrix metalloproteinase type 13 (MMP13), vascular endothelial growth factor (VEGF), and Sox9 were constitutionally expressed and their expression level remained unchanged. We then performed RT-PCR analysis to investigate the expression of chondrocyte-specific genes in chondrocytes treated by nicotine for four months. Nicotine dose-dependently decreased the expression of Col II, Aggrecan, Col X, ALP, and Ihh gene (Figure 3C). These findings suggest that nicotine suppresses matrix synthesis and hypertrophic maturation of chondrocytes in long-term culture using alginate beads.

Functional calcium imaging

To investigate the intracellular signals after nicotinic stimulation, we performed calcium imaging assay for primary chondrocyte cultures, since alpha7 nAChR has large Ca^{2+} permeabilities and also induces elevated intracellular free calcium by releasing intracellular calcium stores [17]. Nicotine elicited a transient increase of intra-cellular calcium (Figure 4A) in a concentration-dependent manner (Figure 4B). MLA, the specific antagonist of alpha7 nAChR, inhibited the calcium signals in a concentration-dependent manner (Figure 4C), implying that the effect of nicotine on chondrocytes is mediated through the alpha7 nAChR.

Maternal nicotine exposure in wild-type mice

To study the effect of nicotine on endochondral ossification in vivo, ovulation-controlled pregnant C57BL/6J mice were given drinking water with or without nicotine during pregnancy, and skeletal growth of their fetuses was observed. At noon on gestational day 15, fetuses were surgicallly obtained and their legs were sectioned for measurement of the femur length (FL) and the length of the hypertrophic zone of the femur (HL) (Figure 5A). There were no significant differences of the amount of water consumed between nicotine-exposed group and control group. Maternal nicotine exposure significantly reduced the FL (Figure 5B) and HL/FL (Figure 5C) of mice at embryonic day 15.5 (E15.5), suggesting that nicotine delayed endochondral ossification.

Maternal nicotine exposure in alpha7 nAChR-disrupted mice

To clarify an involvement of alpha7 nAChR in nicotine-induced delayed skeletal growth in vivo, we investigated the effect

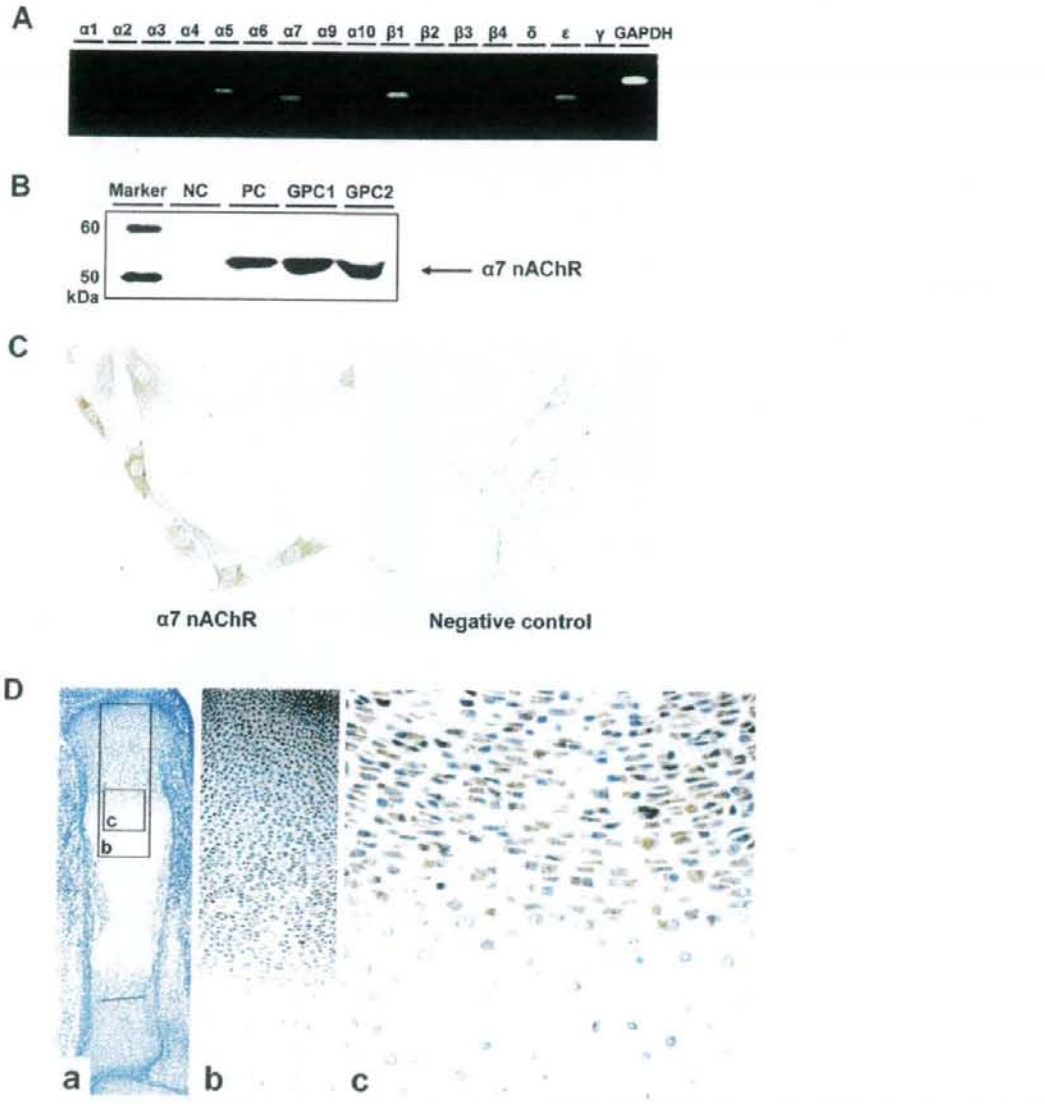

Figure 1. Detection and localization of nAChR subunits in growth plate chondrocytes. A: The expression of each subunit of nAChR. Total RNA was isolated from primary culture of human growth plate chondrocytes. The primers for each subunit are listed in Tables S1–S3. RT-PCR amplified products of alpha5, alpha7, beta1 and epsilon subunits of nAChR and GAPDH. B: Western blot analysis of alpha7 subunit of nAChR in primary chondrocyte cultures. NC: negative control (adipocyte), PC: positive control (PC-12 cell), GPC1,2: human growth plate chondrocyte derived from extra fingers of two individuals. C: Immunocytochemical analysis of alpha7 nAChR subunit in human growth plate chondrocytes. Primary chondrocytes were stained with alpha7 nAChR subunit-specific antibody. D: Immunohistochemical analysis of alpha7 nAChR subunit in tibia of E15.5 fetuses. Alpha7 nAChR are detected at resting, proliferating and pre-hypertrophic chondrocytes of murine growth plate.
doi:10.1371/journal.pone.0003945.g001

of maternal nicotine exposure on skeletal development of murine fetuses in which the alpha7 nAChR gene is disrupted. Maternal genotype is alpha7 nAChR +/− in this experiment (Figure 6), unlike the experiment using wild type mice (Figure 5, maternal genotype: alpha7 nAChR +/+), and littermate fetuses (alpha7 nAChR −/− and alpha7 nAChR +/+) were compared to exclude the effect of nicotine on maternal bodies. Nicotine significantly reduced FL and HL/FL in alpha7 nAChR +/+ fetuses but not in alpha7 nAChR −/− fetuses (Figure 6A, B). However, nicotine did not significantly affect body weight (BW) in both genotypes

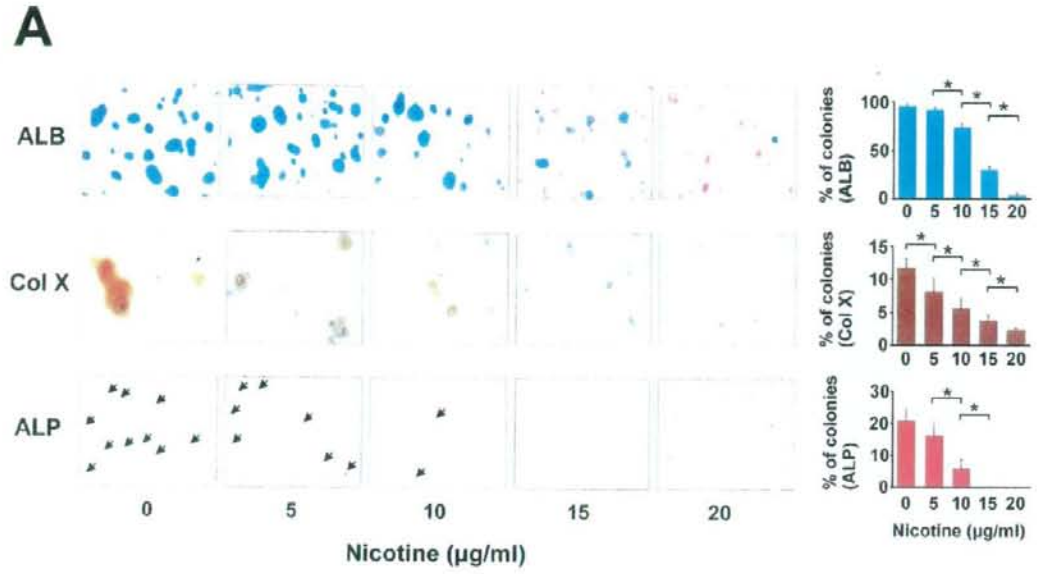

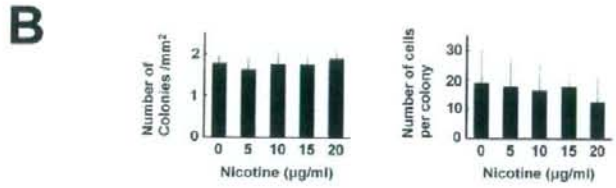

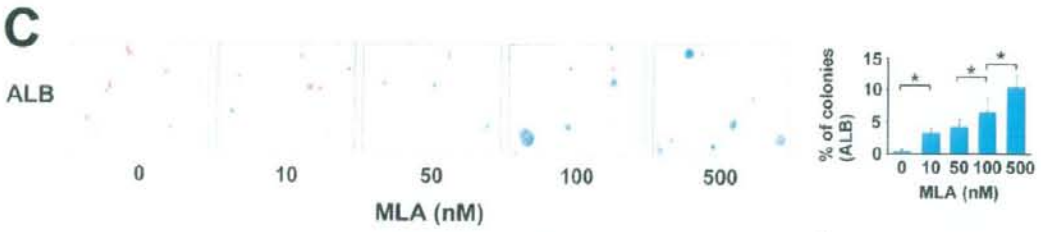

Figure 2. Effect of nicotine on growth plate chondrocytes in agarose gel. Growth plate chondrocytes were cultured in an agarose gel using the modified method previously described [28], and exposed to nicotine and MLA, a specific antagonist for alpha7 nAChR, at the indicated concentration. After three weeks of cultivation, suspension agarose was transferred to a glass slide and the following histological analyses were then performed. A: Microscopic appearance of chondrocyte colonies. From top to bottom: ALB (Alcian blue stain), Col X (immunocytochemistry by an anti-Col X antibody), ALP (enzyme cytochemistry of alkaline phosphatase). For ALB and Col X stain, the slides were counterstained with kernechtrot and hematoxylin, respectively. Percentage of ALB- stained, Col X- positive, and Alkaline phosphatase- positive colonies were counted (right panel, from top to bottom). All the ALP positive colonies in the panels are indicated by arrowheads. Nicotine concentration-dependently suppressed the percentage of the colonies stained with ALB, Col X, and ALP. *, statistically significant, $P<0.02$. B: Number of colonies and number of cells per colony. The number of colonies with a diameter greater than 50 μm (left panel) and cell number per colony (right panel) were counted on the ALB- stained agarose gel slides. C: Microscopic appearance of chondrocyte colonies stained with ALB. MLA reversed the decrease of ALB- positive matrix in a concentration-dependent manner under constant nicotine concentration (20 μg/ml). The percentage of ALB-positive colonies exceeded 10% by using 500 nM MLA. *, statistically significant, $P<0.02$.

doi:10.1371/journal.pone.0003945.g002

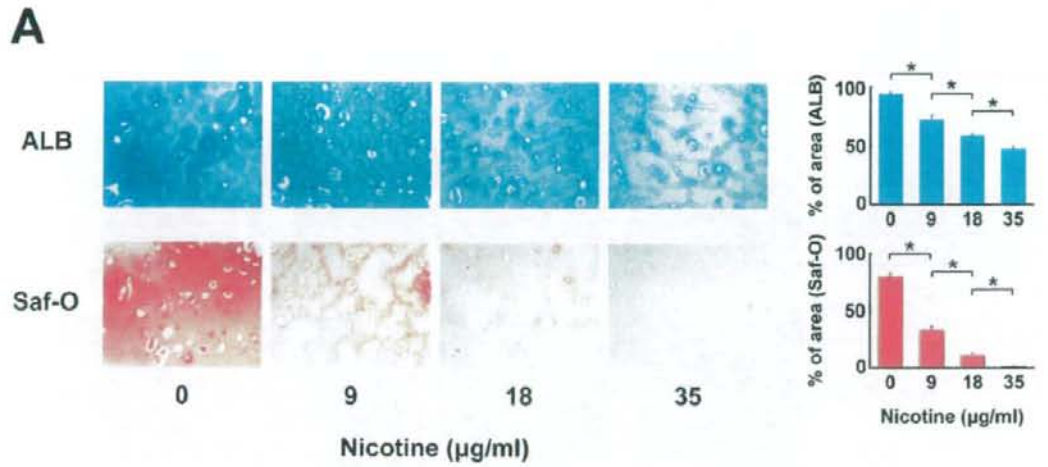

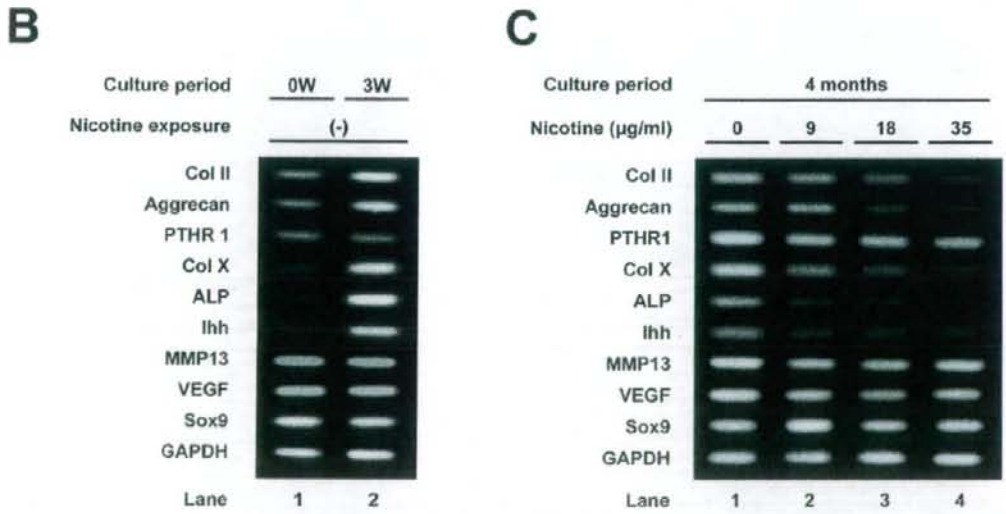

Figure 3. Long-term (four months) effect of nicotine on growth plate chondrocytes in alginate beads. Growth plate chondrocytes in alginate beads were exposed to the indicated concentration of nicotine for four months. A: Microscopic view of chondrocytes in alginate beads after four-months cultivation. Upper panels: ALB stain, lower panels: Safranin-O stain. Chondrocytes were surrounded by matrix which they secreted. Nicotine decreased the area stained with ALB or Safranin-O in a concentration-dependent manner. *, statistically significant, $P<0.02$. B: RT-PCR analysis of chondrocyte-specific gene expression in the chondrocytes at the start of cultivation (lane 1: 0W) and three weeks (lane 2: 3W). From top to bottom: genes for Col II, Aggrecan, parathyroid hormone receptor type 1 (PTHR1), Col X, alkaline phosphatase (ALP), Indian hedgehog (Ihh), matrix metalloproteinase type13 (MMP13), vascular endothelial growth factor (VEGF), Sox9 and GAPDH. C: RT-PCR analysis of chondrocyte-specific gene expression in chondrocytes embedded in alginate beads exposed to the indicated concentration of nicotine for four months. Expression of early stage matrix-gene (Col II and Aggrecan) and markers of hypertrophic chondrocytes (Col X, ALP and Ihh) increased after three weeks of cultivation (B). Nicotine decreased the expression of these genes in a concentration-dependent manner, but had little effect for the expression of MMP13, VEGF, and control genes (Sox9 and GAPDH) (C).
doi:10.1371/journal.pone.0003945.g003

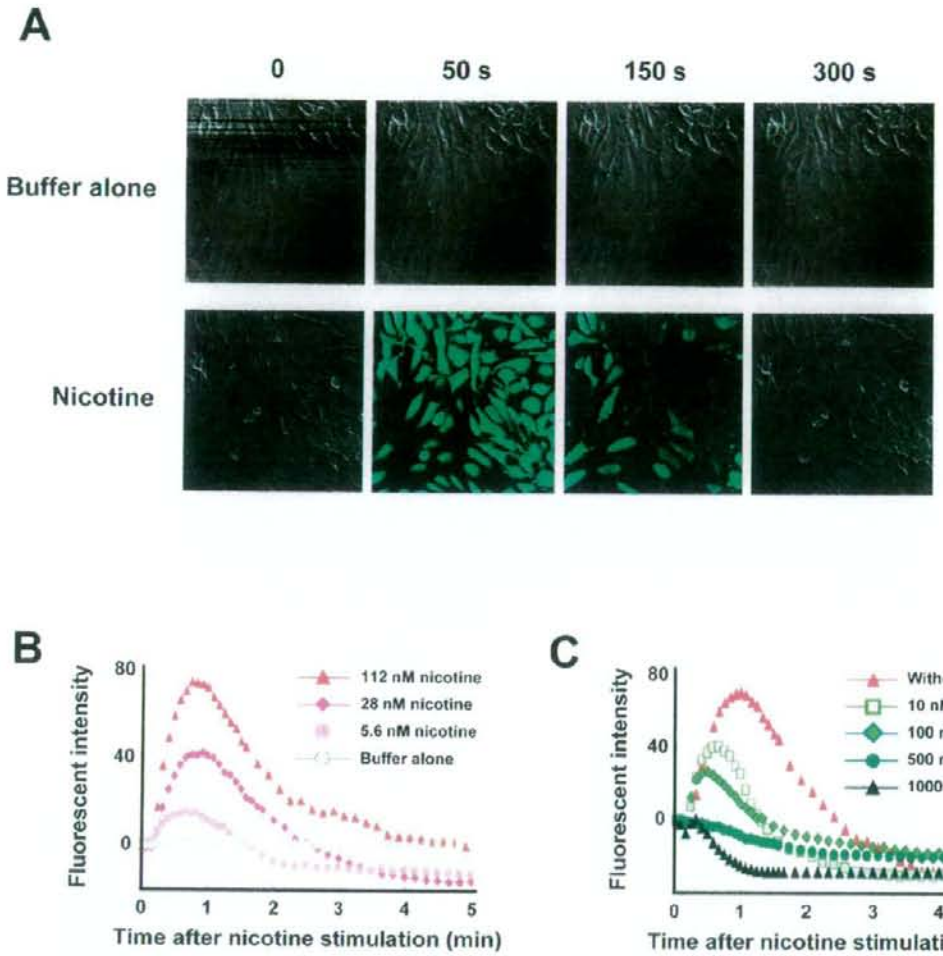

Figure 4. Calcium influx assay in primary chondrocyte culture. Nicotine-stimulated calcium signaling was investigated by the use of a fluorescent Ca^{2+} indicator. Primary chondrocyte cultures were stimulated by nicotine with or without MLA, the specific antagonist of alpha7 homomeric nAChR. A: Addition of assay buffer alone elicits no reaction (upper panels: negative control). Nicotine elicits a transient increase of intracellular calcium (lower panels). B: Nicotine elicits a transient increase of intra-cellular calcium in a concentration-dependent manner. C: MLA inhibits nicotine-induced calcium influx in a concentration-dependent manner. The cells were treated with MLA 30 min before nicotine stimulation.
doi:10.1371/journal.pone.0003945.g004

(Figure 6C). Besides, scatterplot and correlation between the FL and the BW revealed that nicotine downwardly shifted the linear slope in alpha7 nAChR +/+ fetuses but had no effect in alpha7 nAChR −/− fetuses (Figure 6D). These findings suggest that maternal nicotine exposure decreased the fetal endochondral ossification through the fetal alpha7 nAChR in vivo.

Discussion

Alpha7 nAChR was originally identified as a subunit of neuronal nAChR, and has also been shown to be functional in both neuronal and non-neuronal, i.e., non-excitable cells such as lymphocytes, vascular endothelial cells, keratinocytes and bronchial epithelium [16]. In this study, we demonstrated the expression of the alpha7 subunit of nAChR at resting to pre-hypertrophic chondrocytes in murine growth plate and on a culture of human growth plate chondrocytes, and the involvement of alpha7 nAChR in nicotine-induced delayed skeletal growth. The novel findings of alpha7 nAChR in chondrocytes suggest that the effect of smoking on delayed skeletal growth is directly correlated with nicotinic action on chondrocytes.

Direct effect of nicotine on human growth plate chondrocytes

Maternal nicotine exposure decreases the width of the hypertrophic zone of growth plate, increases apoptotic chondrocytes, and reduces the length of femur in rat [20]. Contrarily, nicotine has been shown to up-regulate glycosaminoglycan and

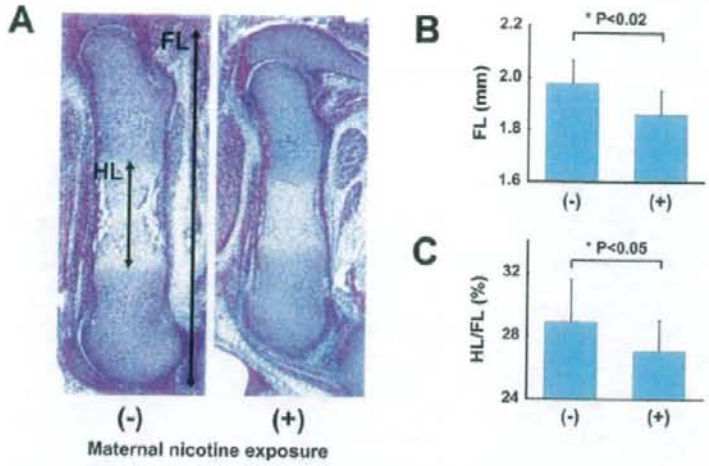

Figure 5. Maternal nicotine exposure in wild-type mice. Ovulation-induced pregnant mice were mated and were given drinking water with nicotine during pregnancy. At noon on gestational day 15, the fetuses were sacrificed, and their legs were histologically investigated. A: Skeletal growth estimated by measuring the femur length (FL) and the length of the hypertrophic zone of the femur (HL). B: FL (mm), C: HL/FL (%) of E15.5 fetuses whose mothers were given drinking water with or without nicotine. Nicotine significantly decreased FL and HL/FL.
doi:10.1371/journal.pone.0003945.g005

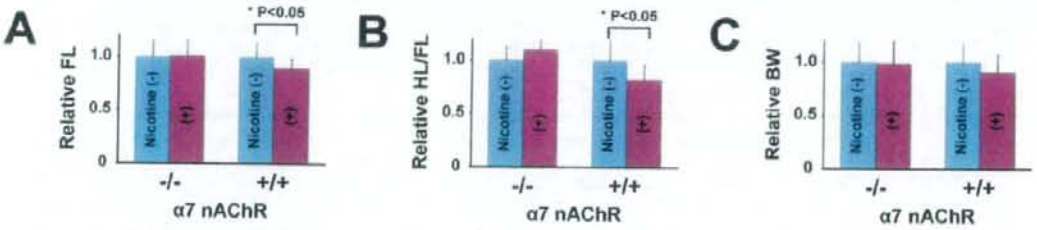

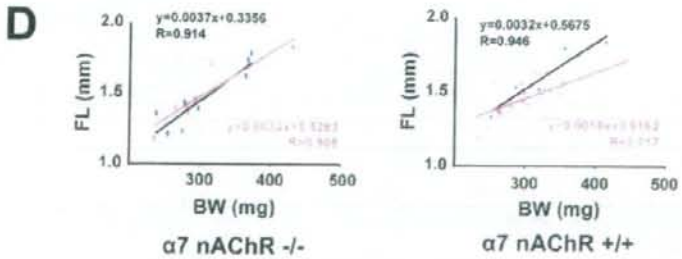

Figure 6. Maternal nicotine exposure in alpha7 nAChR-disrupted mice. A–C: FL, HL/FL, and body weight (BW) of alpha7 nAChR −/− and alpha7 nAChR +/+ E15.5 littermate fetuses. Alpha7 nAChR +/− female were mated with alpha7 nAChR +/− male, and given drinking water with or without nicotine during pregnancy. Relative FL, HL/FL, and BW were calculated, each value in mice that did not receive nicotine was regarded as equal to 1.0. Nicotine significantly reduced FL and HL/FL in alpha7 nAChR +/+ fetuses but not in alpha7 nAChR −/− fetuses (A,B). Nicotine did not significantly reduce BW in either genotype (C). D: Scatterplot and correlation between the FL and BW of mice with (red line) or without (black line) exposure to nicotine. In alpha7 nAChR +/+ fetus, Nicotine downwardly shifts the linear slope in alpha7 nAChR +/+ fetuses but not in alpha7 nAChR −/− fetuses.
doi:10.1371/journal.pone.0003945.g006

collagen synthesis of human articular chondrocytes in vitro [21]. Cultured human growth plate chondrocytes derived from infant fingers serve as a good model for analyzing whether nicotine has direct action on growth plate chondrocytes. The present findings of nicotinic effect, i.e. decreasing matrix synthesis and suppressing hypertrophic differentiation but not proliferation on growth plate chondrocytes in vitro, indicate the direct effect of nicotine on growth plate chondrocytes. The findings are consistent with reports that maternal nicotine exposure has a negative effect on endochondral ossification in animals [13]. Besides, these findings are consistent, considering the fact that longitudinal skeletal growth is partly caused by matrix synthesis and hypertrophic differentiation of chondrocytes. Confirmation of the animal model using "human" chondrocytes is essential since certain chemicals, such as thalidomide, exhibit different effects in humans and rodents.

Differences of expression levels of the genes for Col X, ALP, Ihh, MMP13, and VEGF in alginate beads culture (Figure 3B, C) may attribute to differential regulation among hypertrophic markers. Expression of the Ihh, Col X, and ALP genes were down-regulated by nicotine and the MMP13 and VEGF genes remained unaffected. Alternatively, the difference could be a result of chondrocyte culture, that is, artifactual induction ex vivo, and the MMP13 and VEGF genes were indeed expressed at the start of alginate bead culture with chondrocytes at passage 1 (Fig. 3B, lane 1: "0 W"). In contrast, the Col X, ALP, and Ihh genes were appropriately regulated after three-dimensional culture (Figure 3B, lane 2: "3 W"; Figure 3C, lane 1: without exposure to nicotine), as is the case with gene regulation in the growth plate.

Involvement of alpha7 nAChR in delayed endochondral ossification

The alpha7 nAChR-null mice exhibit normal development, including neural tissue, but alpha7 nAChR-null mice lack nicotinic currents in hippocampal neurons [22], and show abnormalities in late-stage keratinocyte development in the epidermis [23]. Lack of phenotypic abnormality in the femur of fetuses (Figure 5B) and adults indicates that ACh signaling through alpha7 nAChR has little involvement in the process of physiological skeletal growth. Results using MLA, the antagonist to alpha7 nAChR, strongly suggest the involvement of alpha7 nAChR in the nicotinic effect on chondrocytes. Such low-molecular weight substances may, however, have additional unclarified action in addition to any "specific" action. The proof of alpha7 nAChR involvement in delayed skeletal growth was strengthened by the in vivo experiments with alpha7 nAChR gene-disrupted mice. Especially so, considering the fact that maternal nicotine exposure caused delayed skeletal growth in only alpha7 nAChR +/+ fetuses compared with their alpha7 nAChR −/− littermates, fetal alpha7 nAChR but not maternal alpha7 nAChR is responsible for the mechanism of nicotine-induced delayed skeletal growth.

Since nicotine exposure has been reported to be epidemiologically and experimentally correlated with maternal effect, i.e., abnormal placental function and blood flow [10], the physiological and pathological function of alpha7 nAChR in growth plate was confirmed by comparing "littermates" of alpha7 nAChR (Figure 6B). This comparison confirms involvement of alpha7 nAChR on the fetus, and eliminates a possibility of maternal effect. Furthermore, decrease of relative femur length (Figure 6C, scatterplot and correlation, right panel, alpha7 nAChR +/+) and lack of nicotinic effect on body weight of alpha7 nAChR fetuses (Figure 6B, right panel, "BW") by maternal nicotine exposure indicate a specific effect of nicotine on bone growth rather than a systemic effect. Therefore, the effect of smoking during pregnancy on skeletal growth may be attributed to this direct action of nicotine on growth plate chondrocytes, at least in part.

Our studies suggest that, from the large number of chemicals associated with cigarette smoking, nicotine may cause delayed skeletal growth and, indeed, amniotic fluid and breast milk both have higher concentrations of nicotine than maternal serum does [24]. In addition, metabolism of nicotine in the fetus and child is much slower than that in adults [25]. We therefore should pay close attention to the effect of smoking, regardless of being active or passive, on growth plate chondrocytes. This nicotinic effect may also extend to the delay of fracture repair or generation of non-union in adults, since the process of bone repair also partly depends on endochondral ossification.

Materials and Methods

Chondrocyte cultures

Human chondrocytes were isolated from epiphysis of extra fingers, which were surgically excised from patients with polydactyly. Ethical approval for tissue collection was granted by the Institutional Review Board of the National Research Institute for Child Health and Development, Tokyo, Japan (#88). Minced tissue was incubated for 1 h at 37°C in 0.08% trypsin in PBS, then for 6 h at 37°C in 0.2% collagenase type 1 (Wako, Osaka, Japan) in Dulbecco's Modified Eagle's medium (DMEM). The released cells were washed and resuspended in DMEM containing 10% fetal bovine serum (FBS, Sanko Junyaku Co., Tokyo, Japan, lot number: 27110307) and plated at a density of 1×10^6 cells per 100 mm dish for primary monolayer cultures, or 1×10^6 cells per 35 mm dish for calcium influx assay and immunocytochemical assay of nAChR. In each experiment, we used one lot of cultured chondrocytes from extra fingers obtained from four patients.

RT-PCR for detection of nAChR subunit

Total RNA was prepared from epiphysis of extra fingers using Isogen (Nippon Gene) according to the manufacturer's recommendations. DNase-treated RNA was reverse transcribed in 20 µl of RT-PCR mix (50 mM Tris, pH 8.3, 3 mM $MgCl_2$, 75 mM KCl, 50 mM dNTPs, 2.5 µM oligo(dT)$_{20}$, 5 mM DTT, 2 U RNaseOUT and 10 U SuperScriptIII (Invitrogen) at 50°C for 1 h. The PCR was performed in a final volume of 50 µl containing 1 µl of the single strand cDNA product, 25 mM TAPS (pH 9.3), 50 mM KCl, 2.0 mM $MgCl_2$, 1 mM β-mercaptoethanol , 200 µM dNTPs, and AmpliTaq Gold (Applied Biosystems) and 20 pmol of each forward (5′) and reverse (3′) primers (Table S1). For each experiment the housekeeping gene GAPDH was amplified with 25–35 cycles to normalize the cDNA content of the samples. The amplification was performed for 30 cycles, with other conditions following polymerase-producing manufacturer's recommendations. Human brain and skeletal muscle RNAs were purchased from Ambion (Austin, TX).

Western blot analysis for detection of nAChR subunit

Total proteins were isolated from primary monolayer cultures using CelLytic™-M Mammalian Cell Lysis/Extraction Reagent (Sigma). The proteins were separated by SDS-PAGE (Bio-Rad) in a 10% acrylamide gel, then blotted at 60 V for 2 h at 4°C onto a nitrocellulose membrane. Non-specific binding was blocked by incubation in TBS containing 10% BSA and 0.05% Tween-20. The membrane was subsequently incubated at 4°C overnight with the monoclonal antibody to nicotinic acetylcholine receptor, alpha7 subunit (Sigma, St-Louis, MO; product number: N 8158) diluted 1:3000. After rinsing, the membrane was incubated for 1 h at room temperature in horseradish peroxidase-conjugated rabbit

anti-rat IgG antibody (Sigma; A 5795) at a dilution of 1:3000 in TBS containing 0.05% Tween-20. After rinsing, the membrane was immersed in ECL solution (GE Healthcare, Buckinghamshire, UK). Then, the blots were visualized by LAS-1000plus IDX2, the luminescent image analyzer (Fuji Photo Film, Japan).

Immunocytochemical and immunohistochemical analysis

Immunocytochemical analysis was performed as previously described [26]. Briefly, dishes were incubated with antibody to alpha7 subunit of nAChR in PBS containing 1% BSA. As a methodological control, the primary antibody was omitted. After washing in PBS, dishes were incubated with horseradish peroxidase (HRP)-conjugated rabbit anti-rat IgG antibody. Staining was developed by using a solution containing diaminobenzidine and 0.01% H_2O_2 in 0.05 M Tris-HCl buffer, pH 6.7.

For immunohistochemical analysis, hind legs of E15.5 C57BL/6J mice were prepared, fixed in 4% paraformaldehyde phosphate buffer solution (Wako) overnight at 4°C, and embedded in paraffin. Immunohistochemical analysis was performed as previously described [27]. Briefly, slides were treated with 0.4% pepsin (DAKO) at 37°C for 30 min, incubated with primary antibody to alpha7 subunit of nAChR(Sigma, product number: N 8158) diluted 1:2000 in PBS containing 1% BSA at room temperature for 3 h, and incubated with simple mouse stain MAX-PO (RAT), a second antibody, at room temperature for 1 h. Staining was developed by using a solution containing diaminobenzidine and 0.01% H_2O_2 in 0.05 M Tris-HCl buffer, pH 6.7. Finally, slides were counterstained with hematoxylin.

Agarose gel cultures

Chondrocytes were cultured in agarose-stabilized suspension using a modified method as previously described [28]. Primary monolayer cultures were trypsinized, re-suspended in agarose gel medium : DMEM/F-12 containing 10% FBS, 100 units/ml penicillin G, 100 mg/ml streptomycin, and 50 mg/ml ascorbate, to a concentration of 2×10^5 cells/ml, then mixed with equal volume of 1% low-temperature melting agarose (Sigma-Aldrich, Steinheim, Germany) in agarose gel medium, giving a final concentration of 1×10^4 cells/ml suspended in 0.5% low-temperature melting agarose in agarose gel medium (suspension agarose). Three milliliters of suspension agarose were added to 60 mm culture plates that were precoated with 2 ml of 1% autoclaved standard agarose (Bio-Rad, Hercules, CA). The gel was allowed to solidify at 4°C before addition of agarose gel medium. Then, culture plates were placed in a 37°C, 5% CO_2 humidified incubator for 21 days, and medium containing indicated concentration of nicotine was replaced once at the beginning of the week. After 21 days, suspension agarose was transferred to a glass slide, and placed on a plate warmer at 50°C with a covering of positively-charged nylon membranes (Roche, Mannheim, Germany). The slides were completely dried in a incubator at 42°C overnight, and fixed in 4% paraformaldehyde for 15 min, and stained with ALB to identify colonies producing glycosaminoglycans and to observe histologically. Colonies were defined as a cluster of cells with a diameter greater than 50 μm. ALP activity was determined in non-fixed agarose slide by Histofine, ALP substrate kit (Nichirei, Tokyo, Japan) following the manufacturer's product information. Type 10 collagen expression was also determined in the agarose slide using specific monoclonal antibody (Sigma; product number: C7974). The slide was fixed in acetone (Nacalai Tesque, Kyoto, Japan) at room temperature for 20 min. Non-specific binding was blocked with 2.5% normal rabbit serum (DakoCytomation, Glostrup, Denmark) in PBS containing 1% BSA and 1% Triton X-100. Slides were incubated for 6 h at room temperature with primary antibody, diluted 1:2000 in PBS containing 1% BSA. Bound antibody was detected by HRP-conjugated polyclonal rabbit anti-mouse IgM antibody (Dako, Glostrup, Denmark; product number: P 0260) diluted 1:100 in PBS at room temperature for 30 min. Peroxidase activity was visualized with diaminobenzidine tetrahidrochloride plus 0.03% H_2O_2, and slide was counterstained with hematoxylin.

Alginate bead cultures

Chondrocytes were cultured in alginate beads following the method described by De Ceuninck et al. Primary monolayer cultures were trypsinized, washed, and centrifuged. The isolated chondrocytes were suspended at a concentration of 2×10^6 cells/ml in a 1.25% alginate in 0.15 M NaCl. The cell suspension was slowly expressed through a 21 gauge needle and dropped into a 102 mM $CaCl_2$ solution. The beads with approximately 25,000 cells/bead were allowed to polymerize for 10 min and washed three times with 0.15 M NaCl, followed by two washes in DMEM/F12. The beads were then transferred to medium (200 beads/10 ml/60 mm culture dish): DMEM/F-12 containing 10% FBS, 50 μg/ml ascorbate, 100 units/ml penicillin G, 100 mg/ml streptomycin. The beads were cultured at 37°C in a 5% CO_2 humidified incubator for four months, and medium with or without nicotine was replaced twice weekly. The beads were transferred to new dishes every other week to avoid the formation of monolayer cultures on the bottom of the dish by chondrocytes escaping from the beads.

For histological analysis, the beads were fixed in 4% paraformaldehyde, 0.1 M cacodylate buffer, pH 7.4, containing 10 mM $CaCl_2$ for 4 h at room temperature, and then washed overnight at 4°C in 0.1 M cacodylate buffer, pH 7.4, containing 50 mM $BaCl_2$. The beads were dehydrated through alcohols and embedded in paraffin. The sections were routinely stained with ALB and safranin-O.

For RT-PCR analysis, chondrocytes were separated from the beads by incubating the beads in dissolution solution (at a ratio of 200 μl/bead), containing 55 mM EDTA, for 5 min and centrifuged. Total RNA was isolated by using RNeasy (Qiagen) following manufacturer's instructions, and was converted to cDNA by same method as described above. The sequences of PCR primers of human chondrocyte-related gene are listed in Table S2. PCR was performed in a final volume of 50 μl containing 2 μl of the single strand cDNA product (10 ng/μl), 10 mM Tris-HCl (pH8.3), 50 mM KCl, 1.5 mM $MgCl_2$, 200 μM dNTPs, 1.25 U Taq (Takara), and 20 pmol of each forward (5′) and reverse (3′) primers.

Calcium imaging

Primary monolayer cultures in 35 mm glass-bottomed plates were prepared. At near confluence, measurement was done by using Fluo-4 NW calcium assay kit (Molecular Probes, product number: F36206) following the manufacturer's product information. In short, the cells were incubated in dye loading solution containing 2.5 mM probenecid at 37°C for 30 min, then at room temperature for an additional 30 min before nicotine stimulation. The fluorescence was measured in LSM 510 (Carl Zeiss) with the settings appropriate for argon laser. Nicotine and its antagonists were prepared as a solution in assay buffer. If antagonists were used, they were added 30 min prior to nicotine stimulation.

Maternal nicotine exposure in wild-type mice

Three-month-old pregnant mice were purchased at day 1 of pregnancy from Sankyo Laboratories (Tokyo, Japan). The mice were given drinking water containing 2% sucrose (Wako, Osaka, Japan) with or without nicotine (hydrogen tartrate salt; Sigma-

Aldrich, St. Louis, MO). Nicotine was added to the sucrose solution starting at an initial concentration of 25 μg/ml to the treatment group mice. This was increased to 50 μg/ml on days 3 to 4, 100 μg/ml after day 5. The control mice were given only sucrose solution as a drinking water. The pregnant mice were sacrificed at noon on gestational day 15. The embryo were immediately weighed, and the legs were immediately removed and fixed in 4% paraformaldehyde phosphate buffer solution (Wako) for 24 h. Then, the legs were dehydrated through alcohols, embedded in paraffin, and sections were stained with Hematoxylin and Eosin for histological analysis.

Maternal nicotine exposure in alpha7 nAChR-disrupted mice

B6.129S7-Chrna7<tm1Bay>/J, the alpha7 nAChR +/− mice were obtained from Charles River Laboratories Japan. Ten- to 12-week old alpha7 nAChR +/− mice were mated, and pregnant mice were given sucrose solution with or without nicotine. The fetuses were obtained and analyzed as in the case of wild-type C57BL/6J mice, as described above. The alpha7 nAChR genotype was determined by means of PCR reaction with the specific primers (Table S3).

Statistics

The results of the quantative assays were expressed as mean±S.D. Significance was determined with Student's *t* test and ANOVA. All experiments were replicated twice.

Supporting Information

Figure S1 In vivo chondrocytic proliferation assay. A: Paraffin section of the femur of E15.5 C57BL/6J mice immunohistochemically stained with antibody to PCNA. Proliferative chondrocytes extensively stained positive for PCNA regardless of maternal nicotine exposure. B: Percentage of PCNA-positive cells in chondrocytes of the proliferative zone. There is no significant difference between the two groups. Hind legs of E15.5 C57BL/6J mice were prepared, fixed in 4% paraformaldehyde phosphate buffer solution (Wako) overnight at 4°C, and embedded in paraffin. After deparaffinization, slides were autoclaved in 0.01 M citrate buffer (pH 6.0) for 10 min, incubated with primary antibody to PCNA (DAKO: PC10) diluted 1:400 in PBS containing 1% BSA at room temperature for 3 h, and incubated with polyclonal rabbit anti-mouse immunoglobrins/HRP (DAKO: P260) at room temperature for 1 h. Staining was undertaken using a solution containing diaminobenzidine and 0.01% H_2O_2 in 0.05 M Tris-HCl buffer at pH 6.7, followed by counterstaining with hematoxylin.
Found at: doi:10.1371/journal.pone.0003945.s001 (0.06 MB PDF)

Table S1 Primers for nAChR subunit genes
Found at: doi:10.1371/journal.pone.0003945.s002 (0.03 MB PDF)

Table S2 Primers for chondrocyte specific genes
Found at: doi:10.1371/journal.pone.0003945.s003 (0.01 MB PDF)

Table S3 Primers for genotypying alpha7 nAChR gene
Found at: doi:10.1371/journal.pone.0003945.s004 (0.01 MB PDF)

Acknowledgments

We would like to express our sincere thanks to M. Nasu, C-H. Cui, H. Akutsu, K. Miyado, and M. Toyoda for support throughout this work, to H. Abe for providing expert technical assistance, to K. Saito and Y. Ito for their secretarial work, and to A. Crump for reviewing the manuscript.

Author Contributions

Conceived and designed the experiments: AK AU. Performed the experiments: AK HM. Analyzed the data: AK HM AU. Contributed reagents/materials/analysis tools: KS HI ST YT. Wrote the paper: AK AU.

References

1. Davies DP, Abernethy M (1976) Cigarette smoking in pregnancy: Associations with maternal weight gain and fetal growth. Lancet 1: 385–387.
2. Hardy JB, Mellits ED (1972) Does maternal smoking during pregnancy have a long-term effect on the child? Lancet 2: 1332–1336.
3. Wingerd J, Schoen EJ (1974) Factors influencing length at birth and height at five years. Pediatrics 53: 737–741.
4. Karatza AA, Varvarigou A, Beratis NG (2003) Growth up to 2 years in relationship to maternal smoking during pregnancy. Clin Pediatr (Phila) 42: 333–341.
5. Sexton M, Hebel JR (1984) A clinical trial of change in maternal smoking and its effect on birth weight. Jama 251: 911–915.
6. Yerushalmy J (1971) The relationship of parents' cigarette smoking to outcome of pregnancy–implications as to the problem of inferring causation from observed associations. Am J Epidemiol 93: 443–456.
7. Olsen J, Pereira Ada C, Olsen SF (1991) Does maternal tobacco smoking modify the effect of alcohol on fetal growth? Am J Public Health 81: 69–73.
8. Trygg K, Lund-Larsen K, Sandstad B, Hoffman HJ, Jacobsen G, et al. (1995) Do pregnant smokers eat differently from pregnant non-smokers? Paediatr Perinat Epidemiol 9: 307–319.
9. Haddow W Jr, Nesbitt RE, Garcia R (1961) Smoking and pregnancy: carbon monoxide in blood during gestation and at term. Obstet Gynecol 18: 262–267.
10. Mochizuki M, Maruo T, Masuko K (1985) Mechanism of foetal growth retardation caused by smoking during pregnancy. Acta Physiol Hung 65: 295–304.
11. Nordstrom ML, Cnattingius S (1996) Effects on birthweights of maternal education, socio-economic status, and work-related characteristics. Scand J Soc Med 24: 55–61.
12. Man G (1976) Letter: Smoking and the fetus. Lancet 1: 972.
13. Nehon E, Jodscheit K, Guo Y (1999) Maternal passive smoking during pregnancy and fetal developmental toxicity. Part 1: gross morphological effects. Hum Exp Toxicol 18: 232–236.
14. El-Zawawy HB, Gill CS, Wright RW, Sandell LJ (2006) Smoking delays chondrogenesis in a mouse model of closed tibial fracture healing. J Orthop Res 24: 2150–2158.
15. Olsen J (1992) Cigarette smoking in pregnancy and fetal growth. Does the type of tobacco play a role? Int J Epidemiol 21: 279–284.
16. Sharma G, Vijayaraghavan S (2002) Nicotinic receptor signaling in nonexcitable cells. J Neurobiol 53: 524–534.
17. Arneric SP, Brioni JD (1999) Neuronal nicotinic receptors : pharmacology and therapeutic opportunities. New York; Wiley-Liss, xii, 421 p.
18. Tacchetti C, Quarto R, Nitsch L, Hartmann DJ, Cancedda R (1987) In vitro morphogenesis of chick embryo hypertrophic cartilage. J Cell Biol 105: 999–1006.
19. Hauselmann HJ, Fernandes RJ, Mok SS, Schmid TM, Block JA, et al. (1994) Phenotypic stability of bovine articular chondrocytes after long-term culture in alginate beads. J Cell Sci 107 (Pt 1): 17–27.
20. Kurnoth S, Gunes T, Koklu E, Bastug O, Cansiz O, et al. (2007) Influence of maternal nicotine exposure on neonatal rat bone: protective effect of pentoxifylline. Exp Biol Med (Maywood) 232: 398–405.
21. Gullahorn L, Lippiello L, Karpman R (2005) Smoking and osteoarthritis: differential effect of nicotine on human chondrocyte glycosaminoglycan and collagen synthesis. Osteoarthritis Cartilage 13: 942–948.
22. Orr-Urtreger A, Goldner FM, Saeki M, Lorenzo I, Goldberg L, et al. (1997) Mice deficient in the alpha7 neuronal nicotinic acetylcholine receptor lack alpha-bungarotoxin binding sites and hippocampal fast nicotinic currents. J Neurosci 17: 9165–9171.
23. Arredondo J, Nguyen VT, Chernyavsky AI, Bercovich D, Orr-Urtreger A, et al. (2002) Central role of alpha7 nicotinic receptor in differentiation of the stratified squamous epithelium. J Cell Biol 159: 325–336.
24. Luck W, Nau H, Hansen R, Steldinger R (1985) Extent of nicotine and cotinine transfer to the human fetus, placenta and amniotic fluid of smoking mothers. Dev Pharmacol Ther 8: 384–395.

25. Dempsey D, Jacob P 3rd, Benowitz NL (2000) Nicotine metabolism and elimination kinetics in newborns. Clin Pharmacol Ther 67: 458–465.
26. Sano M, Umezawa A, Abe H, Akatsuka A, Nonaka S, et al. (2001) EAT/mcl-1 expression in the human embryonal carcinoma cells undergoing differentiation or apoptosis. Exp Cell Res 266: 114–125.
27. Sano M, Umezawa A, Suzuki A, Shimoda K, Fukuma M, et al. (2000) Involvement of EAT/mcl-1, an anti-apoptotic bcl-2-related gene, in murine embryogenesis and human development. Exp Cell Res 259: 127–139.
28. Benya PD, Shaffer JD (1982) Dedifferentiated chondrocytes reexpress the differentiated collagen phenotype when cultured in agarose gels. Cell 30: 215–224.

MOLECULAR AND CELLULAR BIOLOGY, Apr. 2008, p. 2125–2137
0270-7306/08/$08.00+0 doi:10.1128/MCB.00740-07

Vol. 28, No. 7

Inducible Expression of Chimeric EWS/ETS Proteins Confers Ewing's Family Tumor-Like Phenotypes to Human Mesenchymal Progenitor Cells▽†

Yoshitaka Miyagawa,[1] Hajime Okita,[1]* Hideki Nakaijima,[1] Yasuomi Horiuchi,[1] Ban Sato,[1] Tomoko Taguchi,[1] Masashi Toyoda,[3] Yohko U. Katagiri,[1] Junichiro Fujimoto,[2] Jun-ichi Hata,[1] Akihiro Umezawa,[3] and Nobutaka Kiyokawa[1]

Department of Developmental Biology, National Research Institute for Child Health and Development, 2-10-1, Okura, Setagaya-ku, Tokyo 157-8535, Japan[1]; National Research Institute for Child Health and Development, 2-10-1, Okura, Setagaya-ku, Tokyo 157-8535, Japan[2]; and Department of Reproductive Biology, National Research Institute for Child Health and Development, 2-10-1, Okura, Setagaya-ku, Tokyo 157-8535, Japan[3]

Received 27 April 2007/Returned for modification 13 July 2007/Accepted 7 January 2008

Ewing's family tumor (EFT) is a rare pediatric tumor of unclear origin that occurs in bone and soft tissue. Specific chromosomal translocations found in EFT cause EWS to fuse to a subset of ets transcription factor genes (ETS), generating chimeric EWS/ETS proteins. These proteins are believed to play a crucial role in the onset and progression of EFT. However, the mechanisms responsible for the EWS/ETS-mediated onset remain unclear. Here we report the establishment of a tetracycline-controlled EWS/ETS-inducible system in human bone marrow-derived mesenchymal progenitor cells (MPCs). Ectopic expression of both EWS/FLI1 and EWS/ERG proteins resulted in a dramatic change of morphology, i.e., from a mesenchymal spindle shape to a small round-to-polygonal cell, one of the characteristics of EFT. EWS/ETS also induced immunophenotypic changes in MPCs, including the disappearance of the mesenchyme-positive markers CD10 and CD13 and the up-regulation of the EFT-positive markers CD54, CD99, CD117, and CD271. Furthermore, a prominent shift from the gene expression profile of MPCs to that of EFT was observed in the presence of EWS/ETS. Together with the observation that EWS/ETS enhances the ability of cells to invade Matrigel, these results suggest that EWS/ETS proteins contribute to alterations of cellular features and confer an EFT-like phenotype to human MPCs.

Ewing's family tumor (EFT) is a rare childhood cancer arising mainly in bone and soft tissue. Since EFT has a poor prognosis, it is important to elucidate the underlying pathogenic mechanisms for establishing a more effective therapeutic strategy. EFT is characterized by the presence of chimeric genes composed of EWS and ets transcription factor genes (ETS) formed by specific chromosomal translocations, i.e., EWS/FLI1, t(11;22)(q24;q12); EWS/ERG, t(21;22)(q12;q12); EWS/ETV1, t(7;22)(p22;q12); EWS/E1AF, t(17;22)(q12;q12); and EWS/FEV, t(2;22)(q33;q12) (26). The products of these chimeric genes behave as aberrant transcriptional regulators and are believed to play a crucial role in the onset and progression of EFT (3, 36). Indeed, recent studies have revealed that the induction of EWS/FLI1 proteins can trigger transformation in certain cell types, including NIH 3T3 cells (36), C2C12 myoblasts (12), and murine primary bone marrow-derived mesenchymal progenitor cells (MPCs) (6, 45, 52). However, studies have also indicated that overexpression of EWS/FLI1 provokes apoptosis and growth arrest in mouse normal embryonic fibroblasts and primary human fibroblasts (10, 31), hence hampering understanding of the precise role of EWS/ETS proteins in the development of EFT. The function of EWS/ETS proteins would be greatly influenced by cell type, and thus the cells that can originate EFTs might be more susceptible to the tumorigenic effects of EWS/ETS.

Although the cell origin of EFT is still unknown, the expression of neuronal markers in spite of the occurrence in bone and soft tissues has kept open the debate as to a potential mesenchymal or neuroectodermal origin. As described above, ectopic expression of EWS/FLI1 results in dramatic changes in morphology and the formation of EFT-like tumors in murine primary bone marrow-derived MPCs but not in murine embryonic stem cells (6, 45, 52), supporting the notion that MPCs are a plausible cell origin of EFT (45). However, others argue that MPCs cannot be considered progenitors of EFT without further evidence of similarity between human EFT and MPC-EWS/FLI1-induced tumors in mice (29, 46).

The development of experimental systems using murine species is useful for elucidating the mechanisms behind the pathogenesis of EFT. However, several differences between human and murine systems cannot be ignored; these differences include the expression patterns of surface antigens in MPCs, for instance (7, 44, 51, 53). Moreover, human cells are difficult to transform in vitro, and the transformed cells of mice seem to produce a more aggressive tumor than those of hu-

* Corresponding author. Mailing address: Department of Developmental Biology, National Research Institute for Child Health and Development, 2-10-1, Okura, Setagaya-ku, Tokyo 157-8535, Japan. Phone: 81-3-3416-0181. Fax: 81-3-3417-2496. E-mail: okita@nch.go.jp.

† Supplemental material for this article may be found at http://mcb.asm.org/.

▽ Published ahead of print on 22 January 2008.

TABLE 1. Cell lines used in this study and fusion transcript types

Cell line	Diagnosis	Fusion transcript type	Reference
EES-1	EFT	EWS/FLI1 type I	20
SCCH196	EFT	EWS/FLI1 type I	21
RD-ES	EFT	EWS/FLI1 type II	5
SK-ES1	EFT	EWS/FLI1 type II	5
NCR-EW2	EFT	EWS/FLI1 type II	19
NCR-EW3	EFT	EWS/E1AF	19
W-ES	EFT	EWS/ERG	13
NB69	NB		15
NB9	NB		15
GOTO	NB		47
NRS-1	RMS	PAX3/FKHR	40

mans (1). The findings suggest the existence of undefined cell-autonomous mechanisms that render human cells resistant to malignant transformation. Therefore, the use of human cell models is ideal for clarifying how EFT develops. Models of the onset of EFT have been generated using primary fibroblasts (31) and rhabdomyosarcoma cells (23). However, these cell types are not appropriate for studying the origins of EFT, and a model that precisely recapitulates EWS/ETS-mediated EFT formation is required.

UET-13 cells are obtained by prolonging the life span of human bone marrow stromal cells by use of the retroviral transgenes hTERT and E7 (38, 50), retain the ability to differentiate into not only mesodermal derivatives but also neuronal progenitor-like cells, and are considered a good model for studying the cellular events in human MPCs. Therefore, we have examined the biological effect of EWS/ETS in human MPCs by use of UET-13 cells by exploiting tetracycline-inducible systems for expressing EWS/ETS (EWS/FLI1 and EWS/ERG). Here we report that overexpression of EWS/ETS mediates an EFT-like phenotype, including morphology, immunophenotype, and gene expression profile, with enhancement of the Matrigel invasion ability of UET-13 cells.

MATERIALS AND METHODS

Cell cultures and establishment of UET-13TR-EWS/ETS cell lines. UET-13 cells were cultured in Dulbecco's modified Eagle's medium (DMEM) with 10% Tet system approved fetal bovine serum (T-FBS) (Takara) at 37°C under a humidified 5% CO_2 atmosphere. EFT cell lines (EES-1 [20], SCCH196 [21], RD-ES and SK-ES1 [5], NCR-EW2 and NCR-EW3 [19], and W-ES [13]) and neuroblastoma (NB) cell lines (NB69 and NB9 [15] and GOTO [47]) were cultured in RPMI 1640 with 10% FBS. A rhabdomyosarcoma cell line, NRS-1 (40), was cultured in Eagle's minimal essential medium with 10% FBS. The cell lines used in this study are listed in Table 1.

UET-13 cells were seeded at a density of 5×10^4 cells per well in 24-well tissue culture plates 1 day prior to transfection. For introducing the tetracycline-inducible system, UET-13 cells were transfected with pcDNA6-TR (Invitrogen) by use of Lipofectamine 2000 (Invitrogen). After 72 h, the medium was replaced with fresh medium containing 200 μg/ml of blasticidin S (Invitrogen). Individual resistant clones were selected for a month and designated UET-13TR cells. UET-13TR cells were further transfected with pcDNA4-EWS/ETSs constructed as described below, and individual resistant clones were selected in DMEM containing 10% T-FBS and 200 to 300 μg/ml of Zeocin (Invitrogen). The Zeocin-resistant clones were expanded and tested for the induction of EWS/ETS expression upon the addition of tetracycline by use of reverse transcription-PCR (RT-PCR) as described below.

Plasmid construction. A gateway cassette (bases 1 to 1705) was amplified from pBLOCK-iT3-DEST (Invitrogen) by PCR, and the PCR product was inserted into the EcoRV site of pcDNA4-TO (Invitrogen) (termed pcDNA4-DEST). Since the type II EWS/FLI1 is a stronger transactivator than the type I product (32), we used the type II variant in the present study. EWS/ERG was isolated from W-ES, an EFT cell line, joining EWS exon 7 and ERG exon 9. Full-length EWS/FLI1 type II and EWS/ERG cDNAs were amplified from cDNAs prepared from NCR-EW2 and W-ES cells, respectively, by PCR as described below and cloned into the XmnI-EcoRV sites of pENTR11 (Invitrogen). The resulting pENTR11-EWS/ETSs were recombined with pcDNA4-DEST by use of LR recombination reaction as instructed by the manufacturer (Invitrogen) to construct the tetracycline-inducible EWS/ETS expression vector pcDNA4-EWS/ETSs.

Western blot analysis. UET-13 transfectants were cultivated with or without 3 μg/ml of tetracycline for 72 h. Western blot analysis was performed as previously described (37). Briefly, the cell lysates were prepared and separated on a 10% sodium dodecyl sulfate-polyacrylamide gel electrophoresis gel and transferred onto a polyvinylidene difluoride membrane. The membranes were blocked with 5% skimmed milk in phosphate-buffered saline (PBS) containing 0.01% Tween 20 (Sigma) and incubated with primary antibodies. As the primary antibodies, anti-Fli-1, anti-Erg-1/2/3 (Santa Cruz Biotechnology), and anti-actin (Sigma) were used. Horseradish peroxidase-conjugated anti-rabbit or anti-mouse immunoglobulin G (IgG) antibodies (DakoCytomation) were used as secondary antibodies. Blots were detected by chemiluminescence using an ECL Plus Western blotting detection system (GE Healthcare Bio-Science Corp.) and exposed to X-ray film (Kodak) for 5 to 30 min.

MTT assay and detection of apoptosis. Growth curves of UET-13 transfectants were determined using the 3-(4,5-dimethylthiazol-2-yl)-2,5-diphenyltetrazolium bromide (MTT) assay as described previously (18). The apoptosis was detected using an annexin V-fluorescein isothiocyanate (FITC) apoptosis detection kit (Biovision) according to the manufacturer's instructions and analyzed by flow cytometry (Cytomics FC500; Beckman Coulter).

Immunofluorescence analysis. After 1 week of culture in the absence or presence of tetracycline, UET-13 cells and the transfectants were harvested with 0.25% trypsin plus EDTA (IBL). The cells (2×10^5) were incubated with mouse monoclonal antibodies for 20 min. In the case of fluorescence-labeled antibodies, the cells were washed with PBS and then analyzed. In the case of primary unconjugated mouse antibodies, the cells were washed and then incubated with FITC-conjugated goat anti-mouse IgG antibody (Jackson ImmunoResearch Laboratories) for 20 min. Cell fluorescence was detected using a Cytomics FC500 instrument as described previously (27).

Antibodies against the following human antigens were used: CD10, CD13, CD14, CD29, CD34, CD40, CD44, CD45, CD49e, CD54, CD56, CD61, CD90, CD105, CD117, and CD166 from Beckman Coulter; CD73 from BD Biosciences-Pharmingen; CD55 from Abcam; CD59 from Cedarlane Laboratories; and CD133 and CD271 from Miltenyi Biotec GmbH.

Immunocytochemistry. Cells were grown on collagen type I-coated cover glasses (Iwaki). After 72 h with or without tetracycline, cells were fixed for 30 min in 4% paraformaldehyde and permeabilized in PBS containing 0.2% Triton X-100 (Sigma) for 30 min. Subsequently, they were washed with PBS and blocked in PBS containing 0.1% Triton X-100 and 1% bovine serum albumin (Sigma) for 30 min before being incubated with a monoclonal anti-CD99 antibody, i.e., 12E7 (1:100) (DakoCytomation) or O13 (1:200) (Thermo), and polyclonal anti-Fli-1 antibody (1:100) (Santa Cruz) for 1 h. Bound antibodies were visualized with appropriate secondary antibodies, i.e., Alexa Fluor 488 goat anti-mouse IgG (heavy plus light chains) highly cross-adsorbed and Alexa Fluor 546 goat anti-rabbit IgG (heavy plus light chains) highly cross-adsorbed (Invitrogen) for 1 h at 1:300. Nuclei were counterstained with 4′,6′-diamidino-2-phenylindole (DAPI) or propidium iodide (PI) (Sigma). For the visualization of whole cells, cells were treated with Celltracker Blue (Invitrogen) for 30 min and then fixed. Fluorescence was observed and analyzed using a confocal laser scanning microscope and image software (either FV500 from Olympus or LSM510 from Carl Zeiss). Precise measurements of cell size, nuclear size, and the nucleus-to-cytoplasm (N/C) ratio were performed using Image J (16).

RT-PCR analysis. Total RNA was extracted from cells by use of an RNeasy kit (Qiagen) and reverse transcribed using a first-strand cDNA synthesis kit (GE Healthcare Bio-Science Corp). RT-PCR was performed with a HotstarTaq master mix kit (Qiagen). As an internal control, human GAPDH cDNA was also amplified. The sequences of gene-specific primers for RT-PCR were as follows: for EWS/FLI1 (forward), 5′-ATGGCGTCCACGGATTACAGTACCT-3′; for EWS/FLI1 (reverse), 5′-GGGTCTTCTTTGACACTCAATCG-3′; for EWS/ERG (forward), 5′-ATGGCGTCCACGGATTACAGTACCT-3′; for EWS/ERG (reverse), 5′-TTAGTAGTAAGTGCCCAGATGAGAA-3′; for GAPDH (forward), 5′-CCACCCATGGCAAATTCCATGGCA-3′; and for GAPDH (reverse), 5′-TCTAGACGGCAGGTCAGGT/CCACC-3′. PCR products were electrophoresed with a 1% agarose gel and stained with ethidium bromide.

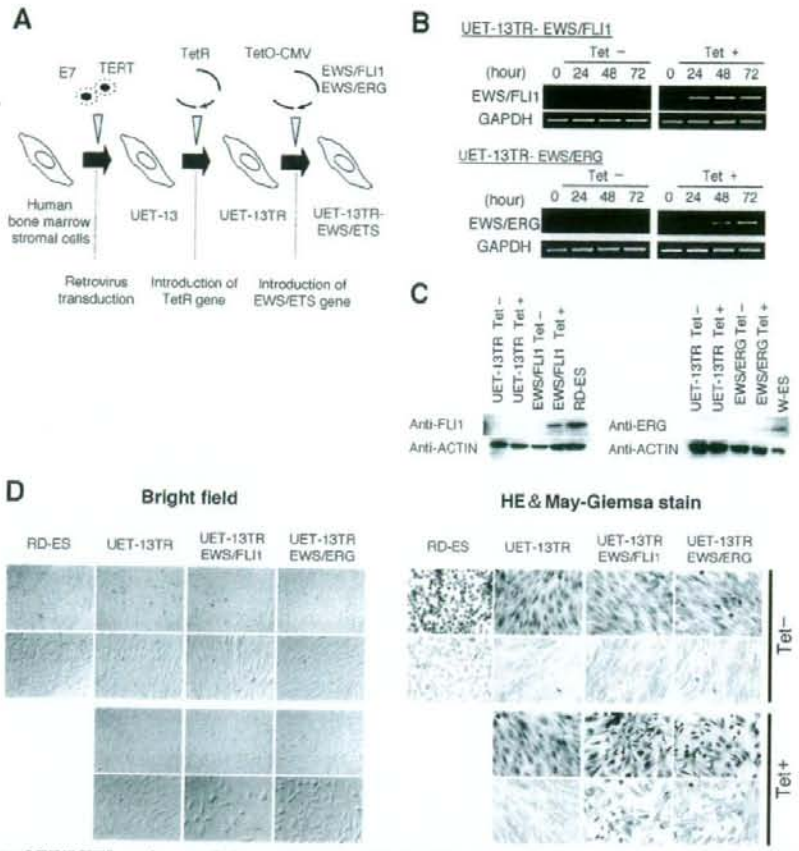

FIG. 1. The effect of EWS/ETS on the morphology of UET-13 cells. (A) The establishment of a tetracycline-inducible EWS/ETS expression system in UET-13 cells. CMV, cytomegalovirus. (B) Analyses for confirming the inducible expression of EWS/ETS genes. EWS/ETS mRNAs were detected in UET-13 transfectants UET-13TR-EWS/FLI1 and UET-13TR-EWS/ERG by RT-PCR. These cells were treated with or without 3 μg/ml of tetracycline (Tet) for the indicated periods. As an internal control, a human GAPDH gene was used. (C) Analyses for confirming the inducible expression of EWS/ETS proteins. The cells were treated as described for panel B and subjected to Western blotting for the detection of EWS/ETS proteins. The extracts of RD-ES and W-ES cells were also examined as positive controls. Membranes were reprobed with anti-actin antibody as a loading control. (D) Morphological change after tetracycline treatment of UET-13 transfectants. UET-13 cells and the transfectants were cultured in the absence or presence of tetracycline for 72 h and observed by light microscopy. Magnification, ×40 (top); ×200 (bottom). Cells were also examined using hematoxylin-eosin (HE) (top) and May-Giemsa (bottom) staining (magnification, ×200).

Real-time RT-PCR. Real-time RT-PCR was performed using TaqMan universal PCR master mix and TaqMan gene expression assays and an inventoried assay on an ABI Prism 7900HT sequence detection system (Applied Biosystems) according to the manufacturer's instructions. The human GAPDH gene was used as an internal control for normalization.

DNA microarray analysis. Total RNA isolated from cells was reverse transcribed and labeled using one-cycle target labeling and control reagents as instructed by the manufacturer (Affymetrix). The labeled probes were hybridized to the human genome U133 Plus 2.0 array (Affymetrix). The arrays were performed in a single experiment and analyzed using GeneChip operating software, version 1.2 (Affymetrix). Background subtraction, normalization, and principal component analysis (PCA) were performed by GeneSpring GX 7.3 software (Agilent Technologies). Signal intensities were prenormalized based on the median of all measurements on that chip. To account for the difference in detection efficiencies between the spots, prenormalized signal intensities on each gene were normalized to the median of prenormalized measurements for that gene. The data were filtered using the following steps. (i) Genes that were scored as absent in all samples were eliminated. (ii) Genes for which the signal intensities were lower than 100 were eliminated. (iii) Performing cluster analysis using filtering genes, we selected the genes that exhibited increased expression or decreased expression in tetracycline-treated cells. Accession numbers for the microarray data are given below.

Invasion assay. The invasion assay was performed using Matrigel (BD Bioscience) according to the previous description (34) with some modification. Polycarbonate filter inserts containing 8-μm pores (BD Falcon) were coated with 50 μl of a 6:1 mixture of culture medium and Matrigel and placed into 24-well culture plates containing DMEM supplemented with 10% T-FBS as chemoattractants. Cells (2.5×10^4) treated with or without tetracycline for 72 h were suspended in DMEM containing 0.01% T-FBS and plated on top of each filter insert. After 20 h in culture in the presence or absence of tetracycline, noninvading cells were removed from upper surface of the filter with a cotton swab. The invading cells on the lower surface of the filter were fixed with formalin, stained with hematoxylin-eosin, and counted in five fields per membrane with light microscopy. As a control, cells were also cultured on uncoated filter inserts. The invasion efficiency was presented as the ratio of the number of invading cells on Matrigel-coated inserts to that on uncoated inserts. Experiments were performed in triplicate, and the means with standard deviations of the values are shown in the graphs in Fig. 8.

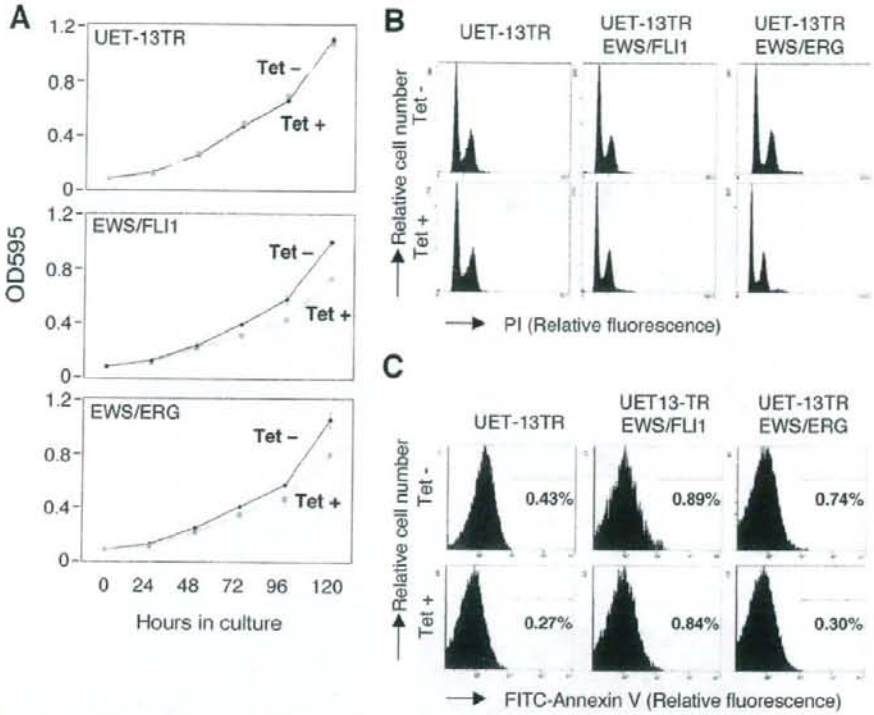

FIG. 2. Effects of EWS/ETS on cell growth in UET-13 cells. (A) Growth curve for UET-13 transfectants. Cells were seeded at 10^3/well and cultured as described for Fig. 1. The increase in cell number was analyzed by MTT assay. Values are means with the standard errors (SE) from three independent experiments. Diamond symbols indicate UET-13 transfectants in the absence of tetracycline (Tet); box symbols indicate UET-13 transfectants in the presence of tetracycline. (B) Cells were cultured as described for panel A in the absence or presence of tetracycline for 3 days and then stained with PI, and DNA contents were analyzed by flow cytometry (*x* axis, relative intensity of fluorescence; *y* axis, relative cell number). (C) Cells treated as described for panel B were stained with FITC-annexin V and analyzed.

Microarray data accession numbers. Microarray data have been deposited in the Gene Expression Omnibus database GEO (www.ncbi.nlm.nih.gov/geo) (accession numbers GSE8665 and GSE8596).

RESULTS

EWS/ETS expression results in morphological changes in UET-13 cells. To investigate how the expression of EWS/ETS affects human MPCs, we used UET-13 cells as a model of human MPCs and expressed EWS/FLI1 (UET-13TR-EWS/FLI1) and EWS/ERG (UET-13TR-EWS/ERG) in a tetracycline-inducible manner (Fig. 1A). As shown in Fig. 1B and C, we confirmed that the tetracycline treatment could induce EWS/ETS expression by RT-PCR analysis and Western blotting. The inducibility upon the addition of doxycycline was comparable to that upon the addition of tetracycline.

Using these cell systems, first we examined the effect of EWS/ETS expression on morphology in UET-13 transfectants. When tetracycline was added to the culture, the morphologies of both UET-13TR-EWS/FLI1 and UET-13TR-EWS/ERG cells were dramatically changed (Fig. 1D). Tetracycline-treated UET-13TR-EWS/ETS cells consisted of a mixture of small round-to-polygonal cells and short spindle cells. The cell morphology resembled that of EFT cell lines. To assess the reproducibility of this phenotypic change, other UET-13TR-EWS/ETS clones were examined, and similar morphological changes were observed. Since tetracycline treatment did not affect the morphology of UET-13TR cells (Fig. 1D), it was suggested that the morphological alteration in UET-13 cells from a mesenchymal cell shape to small round cells, one of the characteristics of EFT, can be attributed to EWS/ETS expression.

EWS/ETS expression inhibits cell growth in UET-13 cells. Next, the effect of EWS/ETS expression on the growth of UET-13 cells was analyzed. As shown in Fig. 2A, an MTT assay revealed that the addition of tetracycline had no effect on the growth of UET-13TR cells but slightly inhibited that of UET-13TR-EWS/ETS cells. We also assessed the cell growth of UET-13 transfectants after tetracycline addition by cell counting and obtained results well in accord with those from the MTT assay (data not shown). To determine the mechanism of this inhibition, DNA content and the binding of annexin V to UET-13 transfectants were examined. No significant increase in either sub-G_1-phase cells (Fig. 2B) or annexin V binding cells (Fig. 2C) was detected, suggesting that EWS/ETS-mediated growth inhibition in UET-13 cells was not due to the activation of an apoptotic pathway. Moreover, no significant decrease in S-G_2-phase cells was observed (Fig. 2B).

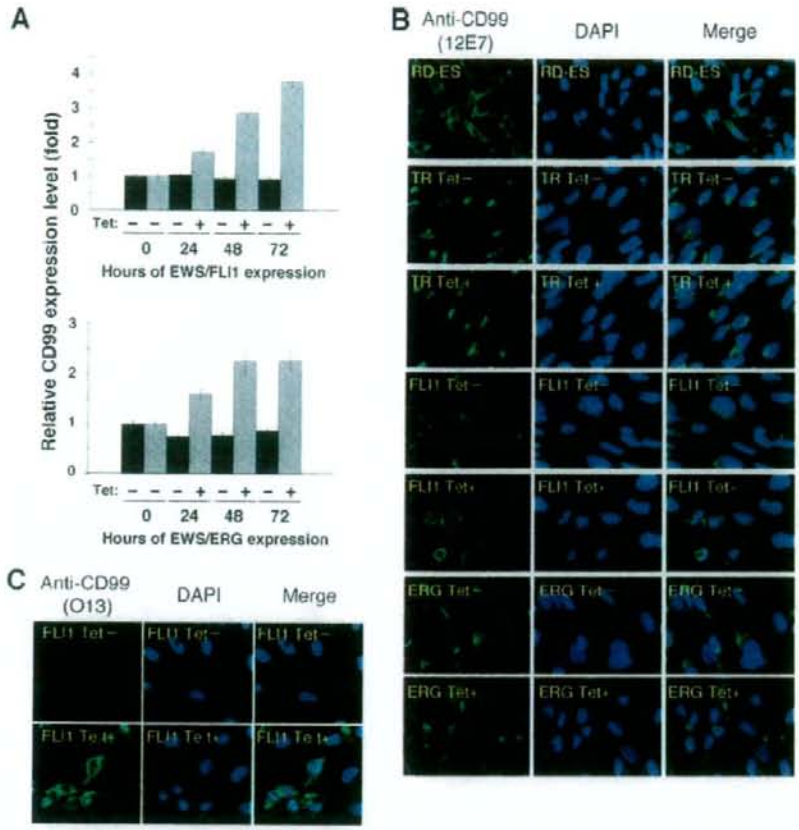

FIG. 3. Effects of tetracycline-mediated EWS/ETS expression on the expression and distribution of CD99 in UET-13 cells. (A) Relative CD99 levels in UET-13 transfectants in the absence or presence of tetracycline (Tet). UET-13 transfectants were treated with or without 3 μg/ml of tetracycline for the indicated periods. Real-time RT-PCR was performed to investigate the expression pattern of CD99. Signal intensities of CD99 were normalized using those of a control housekeeping gene (human GAPDH gene). Data are relative values with standard deviations from triplicate wells and are normalized to the mRNA level at 0 h, which is arbitrarily set to 1 in the graphical presentation. (B and C) Immunocytostaining of CD99 in UET-13 transfectants. Cells were cultured on coverslips in the absence or presence of tetracycline for 72 h and then stained with anti-CD99 antibody 12E7 (B) or O13 (C) as described in Materials and Methods. RD-ES cells were also examined as a positive control. For the staining of nuclei, DAPI was used.

Effect of EWS/ETS on CD99 expression in UET-13 cells. The p30/32MIC-2 gene product, CD99, is a cell surface glycoprotein expressed in EFT with a strong membranous staining pattern and thus constitutes a useful marker for EFT (2, 30). Knowing the dramatic change of morphology in UET-13 cells, we next investigated the mRNA level of CD99 in tetracycline-treated and untreated UET-13 transfectants by quantitative real-time RT-PCR. CD99 levels were clearly elevated by tetracycline treatment in both UET-13TR-EWS/FLI1 and UET-13TR-EWS/ERG cells in a time-dependent manner (Fig. 3A).

We also examined the protein expression of CD99 by immunostaining using 12E7 antibody, which is most widely used as an anti-CD99 antibody. An EFT cell line, RD-ES, showed strong membranous staining of CD99 (Fig. 3B), while neither UET-13TR cells nor UET-13 cells had such a staining. Of note is the fact that although 12E7 reactivity was observed only in the cytoplasm in perinuclear regions in both UET-13TR (Fig. 3B) and UET-13 (data not shown) cells, this antibody is well known to cross-react with a cytoplasmic protein not yet characterized. Since another anti-CD99 antibody, O13, did not react with either UET-13TR (Fig. 3C) or UET-13 (data not shown) cells, we concluded that the perinuclear staining of 12E7 mentioned above was a cross-reaction with unrelated proteins.

In the absence of tetracycline, both UET-13TR-EWS/FLI1 and UET-13TR-EWS/ERG cells were also negative with anti-CD99 antibodies (a pattern designated $CD99^-$), similar to UET-13 cells. Surprisingly, however, tetracycline induced a membranous staining pattern (designated $CD99^+$) in UET-13TR-EWS/FLI1 and UET-13TR-EWS/ERG cells, and some $CD99^+$ cells had irregularly contoured nuclei (Fig. 3B). The same results were observed with another anti-CD99 antibody, O13 (Fig. 3C), indicating that the membranous staining observed for UET-13 transfectants with the anti-CD99 antibodies

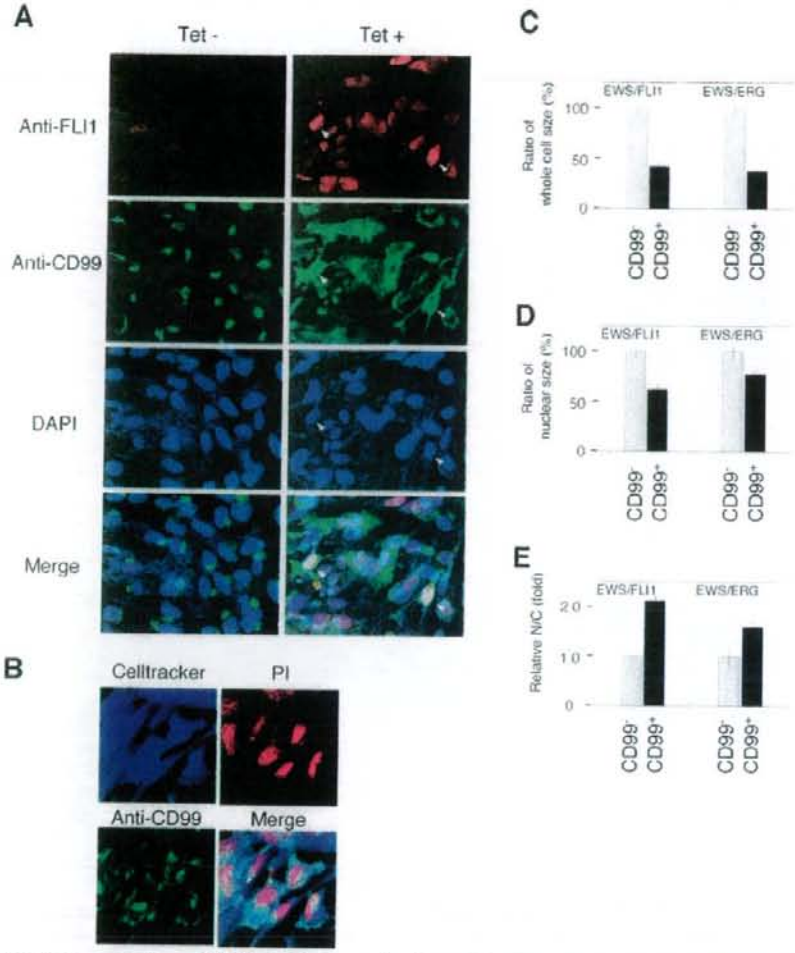

FIG. 4. EWS/ETS expression, alteration of CD99 distribution, and cell morphological changes in UET-13 cells. (A) Immunofluorescence studies using anti-Fli1 (red), anti-CD99 (green), and DAPI (blue). UET-13TR-EWS/FLI1 cells were cultured on coverslips in the absence or presence of tetracycline (Tet) for 72 h and then stained as described in Materials and Methods. White arrowheads indicate $CD99^+$ cells that have a strong staining pattern with anti-Fli1 antibodies and also have remarkable CD99 expression and morphological features. (B) Immunofluorescence analysis by triple staining with whole cells (Celltracker; blue), CD99 (anti-CD99; green), and nuclei (PI; red). UET-13TR-EWS/FLI1 cells were cultured as described for panel A and then stained as described in Materials and Methods. (C to E) Measurements of whole-cell size (C), nuclear size (D), and N/C ratio (E) in tetracycline-treated UET-13 transfectants. UET-13TR-EWS/FLI1 and UET-13TR-EWS/ERG cells were cultured on coverslips in the presence of tetracycline for 72 h and then stained as described in Materials and Methods. These samples were analyzed by the image analysis software Image J ($n = 50$). (C and D) Data are relative values with the SE and are normalized to the size of $CD99^-$ cells, which is arbitrarily set to 100. (E) Data are relative values with the SE and are normalized to the size of $CD99^-$ cells, which is arbitrarily set to 1.

was really CD99 derived. Despite the fact that cells were single colony derived, there was a heterogeneous response to tetracycline treatment in UET-13TR-EWS/FLI1 and UET-13TR-EWS/ERG cells, but most of the $CD99^+$ cells had a small round morphology, one of the characteristics of EFT. To assess the correlation between EWS/FLI1 expression and the change of the CD99 expression pattern, we performed immunofluorescence studies using anti-Fli1 and anti-CD99 antibodies. As shown in Fig. 4A, tetracycline treatment induced a marked enhancement of nuclear staining with anti-Fli1 antibodies in a large number of UET-13TR-EWS/FLI1 cells, indicating the induction of EWS/FLI1 proteins. Furthermore, we observed that the cells with a strong signal for Fli1 tended to reveal a membranous staining pattern with anti-CD99 antibodies and a small round morphology (Fig. 4A). To further verify the correlation between CD99 expression pattern and cell morphology, we estimated the size of cells by triple staining using Celltracker Blue, PI, and anti-CD99 antibody (Fig. 4B). As

TABLE 2. Immunophenotypic characterization of UET-13 transfectants and EFT cells

MPC status[a]	CD marker	Result for[b]: UET-13	UET-13TR		UET-13TR-EWS/FLI1		UET-13TR-EWS/ERG		RD-ES	EFT status[c]	SK-ES1
		Tet$^-$	Tet$^+$	Tet$^-$	Tet$^+$	Tet$^-$	Tet$^+$				
M+	CD29	+	+	+	+	+	+	+	+	+	
M+	CD59	+	+	+	+	+	+	+	+	+	
M+	CD90	+	+	+	+	+	+	+	+	+	E+
M+	CD105	+	+	+	+	+	+	+	+	+	
M+	CD166	+	+	+	+	+	+	+	+	+	
M+	CD44	+	+	+	+	+	+	+	−	−	
M+	CD73	+	+	+	+	+	+	+	−	−	
M+	**CD10**	+	+	+	+	**Down**	+	**Down**	−	−	
M+	**CD13**	+	+	+	+	**Down**	+	**Down**	−	−	
M+	**CD49e**	+	+	+	+	**Down**	+	**Down**	+	−	
M+	**CD61**	+	+	+	+	**Down**	+	**Down**	−	−	
M+	**CD55**	+	+	+	+	**Down**	+	+	+	−	
M+	**CD54**	−	−	−	−	**Up**	−	**Up**	+	+	E+
M(−)	**CD117**	−	−	−	−	**Up**	−	**Up**	+	+	E+
M+/−	**CD271**	−	−	−	−	**Up**	−	**Up**	+	+	E+
	CD40	−	−	−	−	−	−	−	+	+	E+
	CD56	−	−	−	−	−	−	−	+	+	E+
M(−)	CD133	−	−	−	−	−	−	−	+	+	
M(−)	CD14	−	−	−	−	−	−	−	−	−	
M(−)	CD34	−	−	−	−	−	−	−	−	−	
M(−)	CD45	−	−	−	−	−	−	−	−	−	

[a] M(−), negative for MPCs; M+/−, positive for BM-derived MPCs but negative after in vitro culture; M+, positive for MPCs.
[b] +, most cells positive; −, negative; Up, up-regulated by tetracycline treatment; Down, down-regulated by tetracycline treatment. Boldface indicates the antigens the immunophenotypes of which were changed in favor of EFT. Tet$^-$, tetracycline negative; Tet$^+$, tetracycline positive.
[c] E+, positive for EFTs.

presented in Fig. 4C and D, the results clearly showed that the majority of CD99$^+$ cells were significantly smaller in both whole-cell size and nuclear size than the CD99$^-$ cells. Moreover, CD99$^+$ cells also had a substantially increased N/C ratio (Fig. 4E). These results indicated that EWS/ETS expression promoted CD99 expression in UET-13 cells, and CD99 expression status is correlated with the degree of morphological change.

EWS/ETS expression altered the immunophenotype of UET-13 cells. Human MPCs reveal a characteristic expression of several surface antigens and can be identified on the basis of the reactivity with a set of monoclonal antibodies against CD antigens (25, 42). On the other hand, some CD antigens are characteristically expressed on EFT cells (17, 28, 33). Using the combinations of these antibodies listed in Table 2, which are useful for the immunodetection of either MPCs or EFT cells, we further examined whether EWS/ETS expression affects the immunophenotype of UET-13 cells and compared its effect with that on the immunophenotype of EFT cell lines (Table 2 and Fig. 5). As shown in Table 2, UET-13 cells express most of the human primary MPCs markers. Some of the antigens expressed in MPCs, namely, CD29, CD59, CD90, CD105, and CD166, were also found to be expressed in EFT cell lines, but others, namely, CD10, CD13, CD44, CD61, and CD73, were not. In contrast, antigens recognized to be present in EFT cells, including CD40, CD56, and CD133, were absent from UET-13 cells. Interestingly, when the effect of tetracycline-mediated EWS/ETS expression on the immunophenotype of UET-13 cells was tested, levels of some of the antigens present in UET-13 cells, such as CD10, CD13, and CD61, were found to be decreased (Fig. 5). In contrast, some of the markers found in EFT cells, i.e., CD54, CD117, and CD271, became positive in UET-13TR-EWS/ETS cells after tetracycline treatment. Because UET-13TR cells did not show such immunophenotypic change upon treatment with tetracycline, these results indicated that, at least in part, the immunophenotype of UET-13 cells was changed in favor of EFT in the presence of EWS/ETS.

EWS/ETS in UET-13 cells modulates EFT-like gene expression. To further examine the molecular mechanism of EWS/ETS-dependent cellular modulation in human mesenchymal progenitor background, we performed DNA microarray-based expression profiling using the Affymetrix human genome U133 Plus 2.0 array. As a first step to this approach, we validated our experimental systems by analyzing the sequential changes of known EWS/ETS target genes, i.e., inhibitor of differentiation 2 (ID2) (14, 39), NK2 transcription factor related, locus 2 (NKX2.2) (9, 48), and insulin-like growth factor binding protein 3 (IGFBP3) (41). Consistent with previous reports, levels of ID2 and NKX2.2 increased with the expression of EWS/ETS in a time-dependent manner, whereas the expression level of IGFBP3 decreased (Fig. 6A). Employing the same procedure, we also examined whether the change of surface antigen expression was regulated at the transcriptional level and determined the mRNA expression levels of some surface antigens in UET-13 transfectants with or without tetracycline treatment. In accordance with the results of immunocytometric and immunohistological experiments, the mRNA expression levels of CD10, CD13, CD49e, and CD61 were decreased, while those of CD54, CD99, CD117, and CD271 were markedly increased in tetracycline-treated UET-13TR-EWS/ETS cells (Fig. 6B and C), indicating that the expression of these antigens is